J. Fluid Mech. (2020), *vol.* 897, A23.
Published by Cambridge University Press

doi:10.1017/jfm.2020.369

Temperature-gradient-induced massive augmentation of solute dispersion in viscoelastic micro-flows

Siddhartha Mukherjee[1], **Sunando DasGupta**[1,2] **and Suman Chakraborty**[1,3,†]

[1]Advanced Technology Development Center, Indian Institute of Technology Kharagpur, Kharagpur, 721302, India

[2]Department of Chemical Engineering, Indian Institute of Technology Kharagpur, Kharagpur, 721302, India

[3]Department of Mechanical Engineering, Indian Institute of Technology Kharagpur, Kharagpur, 721302, India

(Received 22 September 2019; revised 18 March 2020; accepted 3 May 2020)

Enhancing solute dispersion in electrically actuated flows has always been a challenging proposition, as attributed to the inherent uniformity of the flow field in the absence of surface patterns. Over the years, researchers have focused their attention towards circumventing this limitation, by employing several fluidic and geometric modulations. However, the corresponding improvements in solute dispersion often turn out to be inconsequential. Here we reveal that by exploiting the interplay between an externally imposed temperature gradient, subsequent electrical charge redistribution and ionic motion, coupled with the rheological complexities of the fluid, one can achieve enhancement of up to one order of magnitude of solute dispersion in a pressure-driven flow of an electrolyte solution. Our results demonstrate that the complex coupling between thermal, electrical, hydrodynamic and rheological parameters over small scales, responsible for such exclusive phenomenon, can be utilized in designing novel thermally actuated microfluidic and bio-microfluidic devices with favourable solute separation and dispersion characteristics.

Key words: microfluidics

1. Introduction

Integrating multiple fluidic processes into a single platform has become progressively important in modern lab-on-a-chip devices where separation and mixing often turn out to be two of the most critical processes (Hunter 1981; Probstein 1994; Stroock *et al.* 2002; Ghosal 2004; Stone, Stroock & Ajdari 2004; Masliyah & Bhattacherjee 2006; Whitesides 2006). With the rapid advancement in microfabrication technologies, a large number of research efforts have been dedicated towards developing strategies for improved fluidic mixing or separation (Anderson *et al.* 2000; Glasgow, Batton & Aubry 2004; Karniadakis, Beskok & Aluru 2005; Zhang, He & Liu 2006; Chang & Yang 2008; Sugioka 2010; Ghosh & Chakraborty 2012). Towards achieving enhanced

† Email address for correspondence: suman@mech.iitkgp.ernet.in

mixing in microdevices, diffusion and dispersion are undoubtedly the two most common phenomena. Accordingly, significant research interest in this domain has developed over the past years, with a vision of employing different flow-actuating mechanisms as well as geometric alterations in the fluidic pathways, so as to achieve the desired functionalities.

Although flow actuation using electric fields has wide spectrum of applications in both engineering and medical domains (Becker & Gärtner 2000; Garcia *et al.* 2005; Van Der Heyden, Stein & Dekker 2005; Das, Das & Chakraborty 2006; Das & Chakraborty 2007; Haeberle & Zengerle 2007; Ohno, Tachikawa & Manz 2008; Berli 2010; Mark *et al.* 2010; Zhao 2011; Bandopadhyay & Chakraborty 2012; Nguyen *et al.* 2013; Goswami *et al.* 2015; Das *et al.* 2018), one of the major aspects of the classical electro-osmotic flow in the presence of homogeneous interfacial conditions is the existence of the uniform velocity profile which arises when the electrical double layer (EDL) becomes very thin compared to the channel dimension (Ghosal 2004; Masliyah & Bhattacherjee 2006). This results in a plug-type velocity distribution, thus reducing the extent of mixing significantly.

Hydrodynamic dispersion is the band broadening of a solute which mainly arises from the non-uniformity in the flow field (Taylor 1953; Aris 1956, 1959; Chatwin 1970, 1975; Chatwin & Sullivan 1982; Smith 1982; Barton 1983; Watson 1983; Mazumder & Das 1992; Ng & Yip 2001; Zholkovskij & Masliyah 2004; Ajdari, Bontoux & Stone 2006; Ng 2006; Ghosal 2006; Jansons 2006; Sounart & Baygents 2007; Dutta 2008; Datta & Ghosal 2008; Ghosal & Chen 2012; Arcos *et al.* 2018; Chu *et al.* 2019). Under ideal circumstances, the velocity profile of electro-osmotic flow does not contribute to shear-induced axial dispersion because of the flatness of the velocity profile as opposed to the case of Poiseuille flow (which is parabolic in nature) (Gaš, Štědrý & Kenndler 1997; Ghosal 2004; Mukherjee *et al.* 2019). However, in practice, any inhomogeneity in the flow condition or flow domain can give rise to strong perturbation in the flow field, thereby inducing an axial pressure gradient, which is accompanied by the generation of secondary flow component in order to maintain the flow continuity. In applications demanding augmented dispersion, classical electro-osmotic flow is modulated in two ways, either bringing non-uniformity in the channel geometry or introducing axial variation in the zeta potential (Ajdari 1995, 1996; Ghosal 2002; Mandal *et al.* 2015; Ghosh, Mandal & Chakraborty 2017; Arcos *et al.* 2018).

Over the years, conventional studies of electrokinetics mainly directed their focus towards different techniques of flow actuation, energy conversion and zeta potential measurement under isothermal flow conditions (Levine *et al.* 1975; Zeng *et al.* 2001; Sinton *et al.* 2002; Brask, Kutter & Bruus 2005; Gao *et al.* 2005; Venditti, Xuan & Li 2006; Li, Wong & Nguyen 2009; Mogensen *et al.* 2009; Das & Chakraborty 2010; Bandopadhyay & Chakraborty 2011; Li, Wong & Nguyen 2011). The corresponding literature for non-isothermal flow is relatively scarce because of the lack of understanding of the physics involved. In non-isothermal systems, several complexities come into the picture. First, the modulated thermo-physical properties of an electrolyte solution, like viscosity, electrical permittivity, thermal conductivity, ionic diffusivity and thermophoretic mobility, in the presence of a thermal gradient, strongly influence the fluid motion. Besides this alteration in hydrodynamics, an additional contribution of dielectrophoretic body force due to permittivity variation, accompanied by an induced axial pressure gradient, comes into play in addition to the conventional electrokinetic forcing, thereby bringing complexity to the flow physics (Ghonge *et al.* 2013; Dietzel & Hardt 2017). Additionally, zeta potential, which

plays a crucial dole in governing the flow physics in electrokinetic flows, no longer remains constant in the presence of a thermal gradient (Revil *et al.* 1999; Reppert 2003; Revil, Pezard & Glover 2003; Venditti *et al.* 2006; Ghonge *et al.* 2013). Also, the determination of the temperature field may require a knowledge of other effects like heat generation due to induced streaming field or viscous dissipation which in turn affect fluid physical properties and convective contribution to the temperature distribution. Apart from this, contrary to the conventional electrokinetic studies, the assumption of mechanical equilibrium of ions within the electrical double layer (under isothermal conditions) is no longer valid where the effect of thermo-diffusion of ions needs to be incorporated in the transport equation of ionic species along with other components (Zhou *et al.* 2015; Zhang *et al.* 2019).

The distortion of the local equilibrium of ions in the electrical double layer (EDL) creates a departure from the classical Boltzmann distribution of ions which has direct consequences for the potential distribution. This alteration in charge distribution influences the flow dynamics via electrokinetic forcing, where the intricate coupling between thermal and electrical effects is already prevalent through the aforesaid property variation and an additional dielectrophoretic force. Further, in the absence of any external electric field, the net ionic current turns out to be zero. This condition is itself another source of nonlinearity in the analysis where both conduction and streaming current undergo marked alteration under the influence of finite temperature difference. In addition, it is worth mentioning that, when an electrolyte solution is subjected to an imposed temperature gradient, a thermoelectric field is induced by virtue of the movement of ions in response to the thermal driving force, commonly known as the Soret effect (Ghonge *et al.* 2013; Zhou *et al.* 2015; Dietzel & Hardt 2016, 2017; Zhang *et al.* 2019). Moreover, an additional form of thermoelectric field can be induced within the system because of the diffusivity difference between the ions even if their Soret coefficients remain the same. Besides, the mode of application of thermal gradient can cause significant rearrangement of ions within the EDL and, hence, the subsequent potential distribution for a transverse temperature gradient may not necessarily be the same as that for longitudinal temperature gradient, altering the hydrodynamics in a rather profound manner. Considering the aforementioned intricacies in coupling thermal, electrical and hydrodynamical effects in micro-confinements, research efforts towards addressing various aspects of thermo-solutal convection of electrolyte solutions have turned out to be relatively inadequate, despite having widespread applications in processes like water treatment, charge separation, zeta potential determination, waste heat recovery and energy conversion (Würger 2008, 2010; Sandbakk, Bentien & Kjelstrup 2013; Dietzel & Hardt 2016; Jokinen *et al.* 2016; Barragán & Kjelstrup 2017; Dietzel & Hardt 2017; Li & Wang 2018). As such, the research focus in this domain has been directed primarily towards incorporating non-isothermal effects as a secondary force in the alteration of hydrodynamics of simple fluids (Maynes & Webb 2003; Tang *et al.* 2003; Xuan *et al.* 2004; Chakraborty 2006; Huang & Yang 2006; Xuan 2008; Garai & Chakraborty 2009; Sadeghi *et al.* 2011; Dey, Chakraborty & Chakraborty 2011; Sánchez *et al.* 2018). Therefore, except for some limited physical scenarios, such an exclusive effect has not been utilized to a significant practical benefit (Dietzel & Hardt 2016, 2017; Zhang *et al.* 2019).

Recently, incorporation of a thermal gradient has emerged as an alternative tool in augmenting dispersion where interplay between thermal and electrical effects over small length scales, almost exclusively, dictates the flow physics (Chen *et al.* 2005; Sánchez *et al.* 2018; Mukherjee *et al.* 2019). In addition, it may be noted that with

the emergence of new-generation medical devices, complex bio-fluids have more prominently come into the paradigm of microfluidics (Das & Chakraborty 2006; Berli & Olivares 2008; Olivares, Vera-Candioti & Berli 2009; Berli 2010; Zhao & Yang 2011, 2013). Such fluids exhibit strikingly distinct behaviour compared to the fluids obeying Newton's law of viscosity (Owens 2006; Fam, Bryant & Kontopoulou 2007; Moyers-Gonzalez, Owens & Fang 2008; De Loubens *et al.* 2011; Brust *et al.* 2013; Silva, Alves & Oliveira 2017). Some recent studies have demonstrated that the constitutive behaviour of these biological fluids has close resemblance to the rheology of viscoelastic fluids, and therefore the inclusion of fluid rheology and viscoelasticity in dispersion characteristics has attracted significant attention lately (Brust *et al.* 2013; Arcos *et al.* 2018; Hoshyargar *et al.* 2018; Mukherjee *et al.* 2019). While considering the thermally induced electrokinetic flow of viscoelastic fluids, an additional source of nonlinearity crops up as mediated by the constitutive behaviour of the fluid (Afonso, Alves & Pinho 2009; Coelho, Alves & Pinho 2012; Afonso, Alves & Pinho 2013; Ghosh & Chakraborty 2015; Ferrás *et al.* 2016; Ghosh, Chaudhury & Chakraborty 2016; Mukherjee *et al.* 2017*a*,*b*). Moreover, the degree of viscoelasticity, which is determined using physical properties like fluid viscosity and relaxation time, is a strong function of the prevalent thermal gradient, augmenting the complexity of the problem to a large extent (Bautista *et al.* 2013; Mukherjee *et al.* 2019).

To the best of our knowledge, dispersion characteristics of thermally induced electrokinetic transport of complex fluids in microfluidic environments, where the temperature gradient is solely used for flow manipulation, have not been addressed in the literature. Here, we report the effect of an external temperature gradient on the dispersion characteristics of an electrolyte solution in a parallel-plate microchannel. We subsequently discuss the charge redistribution upon application of the thermal gradient, subsequent perturbation of the fluid motion and its implications for hydrodynamic dispersion, considering both Newtonian and viscoelastic fluids. Our results reveal that by combining some of the electrokinetic, thermal and fluidic parameters coupled with rheological aspects, it is possible to achieve massively augmented solute dispersion, while for some combinations significant enhancement in streaming potential (compared to the solely pressure-driven flow) can also be obtained. We believe that the present analysis can be used as a fundamental basis in the design of thermally actuated micro- and bio-fluidic devices demanding improved solute dispersion where the interplay between electromechanics, thermal effects, hydrodynamics and rheological aspects in narrow confinement can be coupled together to a beneficial effect. Additionally, a wide variety of thermal and fluidic problems can also be approached on the basis of the present theoretical framework (Raj *et al.* 2002; Das, Chakraborty & Dutta 2004; Chakraborty & Chakraborty 2007; Ghatak & Chakraborty 2007; Chakraborty & Srivastava 2007; Chakraborty & Padhy 2008).

2. Problem formulation

We consider non-isothermal electrokinetic flow of a binary 1 : 1 symmetric electrolyte solution through a parallel-plate microchannel. We choose a rectangular Cartesian coordinate system where x and y coordinates represent longitudinal and transverse directions, respectively, while the origin is placed at the centreline of the channel. Length scales in the two directions are l and h, respectively, where the half-channel height (h) is very small compared to the channel length (l), i.e. $h \ll l$ or $\beta = h/l \ll 1$. We have employed two different types of thermal gradients: case 1, axially applied temperature gradient; case 2, temperature gradient applied in the transverse direction (figure 1).

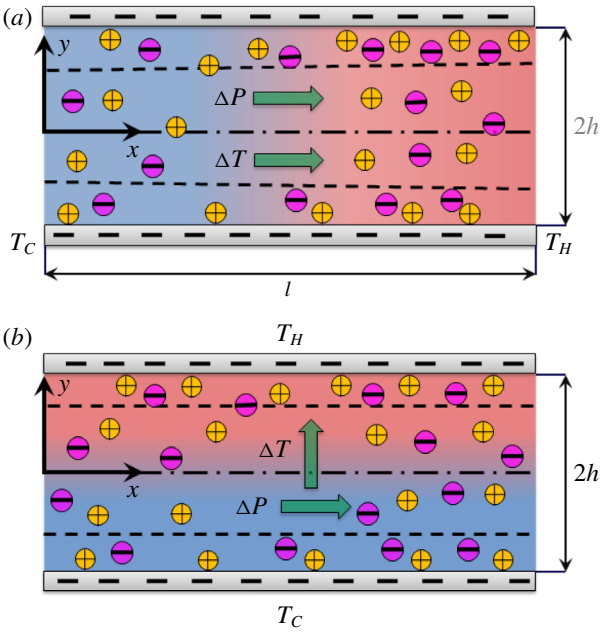

FIGURE 1. Schematic of the combined pressure-driven and temperature-gradient-induced flow of electrolyte solution through a parallel-plate microchannel. (*a*) Temperature gradient is applied in the axial direction. (*b*) Temperature gradient is applied in the transverse direction.

2.1. *Dispersion coefficient: a broad perspective*

We consider the hydrodynamic dispersion characteristics of a combined pressure-driven and thermal-gradient-driven electrokinetic flow of an electrolyte solution. According to the definition of the band-broadening phenomenon, the hydrodynamic dispersion coefficient ($\overline{D}_{eff}$) depends on the rate of change of variance of solute displacement band as $D_{eff} = \frac{1}{2}(\mathrm{d}/\mathrm{d}t)\sigma^2(t)$, where σ^2 is the variance of solute displacement. This temporal variation with respect to the centroid of the band depends on the plate height (h') as $h' = (\mathrm{d}/\mathrm{d}x')\sigma^2(x')$, where x' denotes the location of the band centroid. Knowledge of the plate height is necessary in determining the dispersion coefficient because of its ability to incorporate any change in the variance of the mean concentration. For a band of non-adsorbing solute flowing in a rectangular channel, the velocity of the centre mass becomes equal to the mean axial velocity of flow, i.e. $u_{avg} = \mathrm{d}x'/\mathrm{d}t$. Using the descriptions of h' and x', one can rewrite the expression of the dispersion coefficient as

$$D_{eff} = u_{avg}h'/2. \tag{2.1}$$

Here, u_{avg} is the mean velocity averaged cross-sectionally. As reported in the literature (Van Deemter, Zuiderweg & Klinkenberg 1956), the plate height is related to the mean velocity as

$$h' = 2D/u_{avg} + (u_{avg}h_{min}^2/8D). \tag{2.2}$$

In (2.2), h_{min} is the minimum plate height for a given flow condition and D is diffusivity. On the right-hand side, the contribution of the molecular diffusion is represented by the first term while the second term represents the contribution due to the non-uniformity in the flow field. By following some recent studies (Arcos *et al.*

2018; Hoshyargar *et al.* 2018), we have used the following expression for evaluating h_{min}:

$$h_{min}^2 = \frac{16}{h}\int_0^h \int_0^y [\{(u/u_{avg}) - 1\}\,\mathrm{d}y]^2\,\mathrm{d}y. \tag{2.3}$$

Combining all this, the dimensionless form of the dispersion coefficient ($\overline{D}_{eff}$) reads as

$$\overline{D}_{eff} = 1 + (Pe_D \overline{u}_{avg}\overline{h}_{min})^2/16, \tag{2.4}$$

where Pe_D is the dispersion Peclet number, $\overline{h}_{min} = h_{min}/h$ and $\overline{u}_{avg} = u_{avg}/u_c$ is the dimensionless average flow velocity with u_c being the characteristic velocity scale.

For the sake of brevity, the detailed mathematical expressions for obtaining the hydrodynamic dispersion coefficient are presented in § A of the supplementary material, available at https://doi.org/10.1017/jfm.2020.369, which clearly illustrates the complicated mathematical and physical interplay of the solutal, hydrodynamic and thermal fields, restrained by the consideration of overall electroneutrality. As clear from the definition, the dispersion coefficient depends directly on the velocity field, which in turn is influenced strongly by the charge distribution modulated by external temperature gradient, mediated by a two-way coupling. The governing equations delineating the same are discussed in the subsequent subsection.

2.2. *Governing equations and boundary conditions*

In this section, we first present the governing equation for the temperature distribution. Unlike conventional streaming-field-induced electrokinetic flow, here temperature (T) within the microchannel does not remain constant which is given by the following energy equation:

$$\rho C_p\left(u\frac{\partial T}{\partial x} + v\frac{\partial T}{\partial y}\right) = \frac{\partial}{\partial x}\left(k\frac{\partial T}{\partial x}\right) + \frac{\partial}{\partial y}\left(k\frac{\partial T}{\partial y}\right) + Q_{gen} + Q_{vd}, \tag{2.5}$$

where the left-hand side is the advective contribution, the first two terms on the right-hand side are the conductive contributions, $Q_{gen} = \sigma E_x^2 = (2z^2e^2Dn_\infty/k_BT)(-\partial\phi/\partial x)^2$ is the heat generation term due to the induced streaming field and $Q_{vd} = \mu[2\{(\partial u/\partial x)^2 + (\partial v/\partial y)^2\} + (\partial u/\partial y + \partial v/\partial x)^2] - \frac{2}{3}\mu(\boldsymbol{\nabla}\cdot v)^2$ is the viscous dissipation term with $\mu = \mu_{ref}\exp[-\omega_1(T - T_{ref})]$ being the fluid viscosity. Parameters ρ and C_p are the density and specific capacities of the fluid, $E_x = -\partial\phi/\partial x$ is the induced streaming field and σ is the bulk electrical conductivity, where $\sigma = 2z^2e^2Dn_\infty/k_BT$ with z, e, D, n_∞ and k_B being the valence of ions, elementary electronic charge, average diffusivity of ions, bulk ionic number density and Boltzmann constant, respectively. Using the respective scales of the pertinent variables, the corresponding dimensionless form can be written as

$$\begin{aligned}\beta Pe_T\left(\overline{u}\frac{\partial\theta}{\partial\overline{x}} + \overline{v}\frac{\partial\theta}{\partial\overline{y}}\right) &= \beta^2\frac{\partial}{\partial\overline{x}}\left(\frac{k}{k_{ref}}\frac{\partial\theta}{\partial\overline{x}}\right)\\ &+ \frac{\partial}{\partial\overline{y}}\left(\frac{k}{k_{ref}}\frac{\partial\theta}{\partial\overline{y}}\right) + \beta^2\frac{\varepsilon\kappa^2 D}{k_{ref}\Delta T_{ref}}\left(\frac{k_BT_C}{ze}\right)^2\left(\frac{\partial\overline{\phi}}{\partial\overline{x}}\right)^2\\ &+ \frac{\mu {u_c}^2}{k_{ref}\Delta T_{ref}}\left[2\beta^2\left\{\left(\frac{\partial\overline{u}}{\partial\overline{x}}\right)^2 + \left(\frac{\partial\overline{v}}{\partial\overline{y}}\right)^2\right\} + \left(\frac{\partial\overline{u}}{\partial\overline{y}} + \beta^2\frac{\partial\overline{v}}{\partial\overline{x}}\right)^2\right],\end{aligned} \tag{2.6}$$

where $\overline{u} = u/u_c$ is the dimensionless axial velocity component, $\overline{v} = vl/(u_ch)$ is the dimensionless transverse velocity component, $\theta = (T - T_C)/\Delta T_{ref}$ is the dimensionless temperature, $\overline{\phi} = (ze\phi)/(k_BT_C)$ is the dimensionless potential, $\varepsilon = \varepsilon_{ref}\exp[-\omega_2(T - T_{ref})]$ is the electrical permittivity and $k = k_{ref}\exp[\omega_3(T - T_{ref})]$

is the thermal conductivity of the fluid. Parameters u_c and $T_C = T_{ref}$ are taken as characteristic scales of velocity and temperature with $\Delta T_{ref} = (T_H - T_C)/2$ being the characteristic temperature difference. Here, κ is the inverse of the EDL thickness and Pe_T is the thermal Peclet number $Pe_T = u_c h \rho C_p / k_{ref}$. The assumptions for the simplification of the energy equation are described in detail in § A1 of the supplementary material. For temperature gradient applied in the axial direction, the simplified non-dimensional equation is

$$\frac{\partial}{\partial \bar{x}}\left(\bar{k}\frac{\partial \theta}{\partial \bar{x}}\right) = 0. \tag{2.7}$$

This equation is subjected to a low temperature T_C at the channel entrance (i.e. at $x = 0$) and a high temperature T_H at the channel exit (i.e. at $x = l$).

For the transport of the ionic species, here, in the presence of a thermal gradient, ions no longer remain in equilibrium and one cannot consider a Boltzmann distribution assumption while obtaining the potential distribution. One needs to find the ionic number concentration (n_i) first, which can be obtained by employing the classical Nernst–Planck equation $\boldsymbol{\nabla} \cdot J_i = 0$, where

$$J_i = n_i v - D_i \boldsymbol{\nabla} n_i - n_i D_{Ti} \boldsymbol{\nabla} T - n_i \mu_i{}^* \boldsymbol{\nabla} \phi. \tag{2.8}$$

Here, the ionic flux J_i consists of four components: advective ($n_i v$), diffusive ($D_i \boldsymbol{\nabla} n_i$), thermo-diffusive ($n_i D_{Ti} \boldsymbol{\nabla} T$) and electro-migrative ($n_i \mu_i^* \boldsymbol{\nabla} \phi$) components. Parameter D_i is the diffusivity and D_{Ti} and $\mu_i^* = e z_i D_i/(k_B T)$ are the thermophoretic and electrophoretic mobilities, respectively. The dimensionless form of the Nernst–Planck equation reads as

$$\begin{aligned}\beta^2 Pe_i \left(\bar{u}\frac{\partial \bar{n}_i}{\partial \bar{x}} + \bar{v}\frac{\partial \bar{n}_i}{\partial \bar{y}}\right) = \beta^2 \frac{\partial}{\partial \bar{x}}\left[\frac{D_i}{D}\left(\frac{\partial \bar{n}_i}{\partial \bar{x}} + \bar{n}_i \bar{S}_{Ti}\gamma \frac{\partial \theta}{\partial \bar{x}}\right.\right. \\ \left.\left. + \frac{\bar{z}_i \bar{n}_i}{1+\gamma\theta}\frac{\partial \bar{\phi}}{\partial \bar{x}}\right)\right] + \frac{\partial}{\partial \bar{y}}\left[\frac{D_i}{D}\left(\frac{\partial \bar{n}_i}{\partial \bar{y}} + \bar{n}_i \bar{S}_{Ti}\gamma \frac{\partial \theta}{\partial \bar{y}} + \frac{\bar{z}_i \bar{n}_i}{1+\gamma\theta}\frac{\partial \bar{\phi}}{\partial \bar{y}}\right)\right],\end{aligned} \tag{2.9}$$

where $\bar{S}_{Ti} = (D_{Ti}/D_i) T_C$ is the Soret coefficient of ions, $Pe_i = u_c l/D$ is the ionic Peclet number, $\bar{n}_i = n_i/n_0$ is the non-dimensional ionic number concentration and $\bar{z}_i = z_i/z$ is the dimensionless valence of ions. Potential $\bar{\phi}$ consists of two terms: $\bar{\phi} = \bar{\phi}(\bar{x}) + \psi(\bar{x}, \bar{y})$, where $\bar{\phi}(\bar{x})$ is the induced streaming field with $\bar{\psi}(x, y)$ being the potential induced within EDL. Equation (2.9) is subject to (*a*) the symmetry condition at the channel centreline (at $\bar{y} = 0$, $\partial \bar{n}_i/\partial \bar{y} = 0$) and (*b*) the number density being equal to the bulk number concentration in the electroneutral region (i.e. $\bar{n}_i = \bar{n}_{i\infty}$ at $\bar{\psi} = 0$). Once the ionic number concentration is known, one can obtain the potential distribution using the Poisson equation:

$$\boldsymbol{\nabla} \cdot (\varepsilon \boldsymbol{\nabla} \phi) = -\rho_e = -e \sum_i z_i n_i. \tag{2.10}$$

The simplified form of the potential distribution is given by

$$\bar{\varepsilon}\frac{\partial^2 \bar{\psi}}{\partial \bar{y}^2} = \bar{\kappa}_{eff}^2 \sinh\left(\frac{\bar{\psi}}{1+\gamma\theta}\right). \tag{2.11}$$

The potential distribution described by (2.11) is subject to the temperature-dependent zeta potential boundary conditions at the channel walls (i.e. at $\bar{y} = \pm 1$, $\bar{\psi} = \psi/\zeta = [1 + C_\zeta \gamma \theta]$). The simplifications of the ionic number concentration and subsequent potential distribution are presented in detail in § A2 of the supplementary material.

Now, we first address the flow field for Newtonian fluids, to provide as a basis for comparison. For the same, one can determine the velocity field using the momentum equation where the above-obtained temperature distribution and potential distribution are employed:

$$0 = -\nabla p + \nabla \cdot \mu[\nabla v + (\nabla v)^{\mathrm{T}}] + F_{EK} + F_{DEP}. \tag{2.12}$$

The left-hand side of (2.12) is zero because the flow is in the inertial regime ($Re \ll 1$). Here, p is the hydrodynamic pressure, $\mu[\nabla v + (\nabla v)^{\mathrm{T}}]$ the viscous stress, $F_{EK} = -\rho_e \nabla \phi$ the electrokinetic force and $F_{DEP} = -(1/2)(\nabla \phi)^2 \nabla \varepsilon$ the dielectrophoretic force. The simplifications for the velocity distribution are discussed in detail in § A3 of the supplementary material. The simplified form of the two components of the momentum equation reads as

$$\left.\begin{aligned} x\text{-component}: \quad 0 &= -\frac{\partial \overline{p}}{\partial \overline{x}} + \overline{\mu}\frac{\partial^2 \overline{u}}{\partial \overline{y}^2} + \frac{\lambda \overline{\varepsilon}}{\overline{\kappa}_{eff}^2}\left[\frac{\partial^2 \overline{\psi}}{\partial \overline{y}^2}\frac{\partial \overline{\phi}}{\partial \overline{x}} + \frac{1}{2}\gamma C_\varepsilon \left(\frac{\partial \overline{\psi}}{\partial \overline{y}}\right)^2 \frac{\partial \theta}{\partial \overline{x}}\right], \\ y\text{-component}: \quad 0 &= -\frac{\partial \overline{p}}{\partial \overline{y}} + \frac{\lambda \overline{\varepsilon}}{\overline{\kappa}_{eff}^2}\frac{\partial^2 \overline{\psi}}{\partial \overline{y}^2}\frac{\partial \overline{\psi}}{\partial \overline{y}}. \end{aligned}\right\} \tag{2.13}$$

In (2.13), the parameter λ is the ratio of the induced velocity due to osmotic pressure to the characteristic flow velocity. Now, we use the no-slip condition at the channel wall (i.e. at $\overline{y} = 1$, $\overline{u} = 0$) and symmetry condition at the channel centreline (at $\overline{y} = 0$, $\partial \overline{u}/\partial \overline{y} = 0$) to obtain the velocity profile. For the completeness of the flow field, one needs to evaluate the streaming potential induced by the combined action of imposed pressure gradient and temperature gradient by using the electroneutrality constraint, i.e. $I_{net} = I_{streaming} + I_{advection} = 0$.

The final part of the present study is to highlight the effect of fluid viscoelasticity on the hydrodynamic dispersion coefficient for which the constitutive equation of the simplified Phan-Thien–Tanner (sPTT) model has been used. The stress components of the sPTT model take the following form (Afonso *et al.* 2009; Bautista *et al.* 2013; Arcos *et al.* 2018):

$$\left.\begin{aligned} 2\mu_{eff}\frac{\partial u}{\partial x} &= F\tau_{xx} + \lambda_{eff}\left(u\frac{\partial \tau_{xx}}{\partial x} + v\frac{\partial \tau_{xx}}{\partial y} - 2\frac{\partial u}{\partial x}\tau_{xx} - 2\frac{\partial u}{\partial y}\tau_{yx}\right), \\ 2\mu_{eff}\frac{\partial v}{\partial y} &= F\tau_{yy} + \lambda_{eff}\left(u\frac{\partial \tau_{yy}}{\partial x} + v\frac{\partial \tau_{yy}}{\partial y} - 2\frac{\partial v}{\partial x}\tau_{xy} - 2\frac{\partial v}{\partial y}\tau_{yy}\right), \\ \mu_{eff}\left(\frac{\partial u}{\partial y} + \frac{\partial v}{\partial x}\right) &= F\tau_{xy} + \lambda_{eff}\left(u\frac{\partial \tau_{xy}}{\partial x} + v\frac{\partial \tau_{xy}}{\partial y} - \frac{\partial u}{\partial y}\tau_{yy} - \frac{\partial v}{\partial x}\tau_{xx}\right), \end{aligned}\right\} \tag{2.14}$$

where $F = 1 + \delta\lambda_{eff}(\tau_{xx} + \tau_{yy})/\mu_{eff}$ is the stress coefficient function with δ being the extensibility of the fluid and $\lambda_{eff} = \lambda_{ref}\exp[-\omega_4(T - T_{ref})]$ the fluid relaxation time.

3. Solution methodology

For a temperature gradient applied in the axial direction, we have obtained both exact solutions and approximate analytical solutions, while for a transverse temperature gradient, approximate analytical solution and numerical solution are obtained. For an approximate analytical solution, an asymptotic approach has been followed where any variable φ can be expanded as

$$\varphi = \varphi_0 + \gamma\varphi_1 + \gamma^2\varphi_2, \tag{3.1}$$

where $\gamma = \Delta T/T_C$ is the thermal perturbation parameter which is the ratio of the imposed temperature difference to the cold-side temperature. Therefore, $\gamma \to 0$ represents the isothermal condition. To check the validity of the asymptotic solution, we have compared it with the exact solution (for axial thermal gradient) and numerical solutions (for transverse thermal gradient) and the upper limit of γ has been fixed accordingly. This comparison is shown in § C2 of the supplementary material.

4. Results and discussion

Since this analysis involves a large set of parameters, numerous results can be obtained by combining all pertinent parameters. However, for improved readability, we have highlighted some key results involving velocity distribution, induced streaming potential, volumetric flow rate and finally the dispersion coefficient (which in turn depends on previous parameters). For representing the results, we have employed some dimensionless parameters. These parameters along with their expressions, physical significance and typical ranges are given in table 1.

The reason for choosing the range of the dimensionless parameters is discussed in § C1 of the supplementary material.

4.1. *Effect of axial temperature gradient*

In figure 2, the variation of streaming potential ratio (E_r) is plotted against some key parameters. Here, E_r is defined as the ratio of the streaming potential induced due to the combined action of externally imposed thermal and pressure gradients to that induced due to the sole action of pressure gradient. While realizing the alteration in the flow field upon applying a thermal gradient, one can expect the effect of the electrical permittivity variation induced dielectrophorteic force on the flow field by inducing an axial pressure gradient, i.e. osmotic pressure gradient due to excess charge redistribution. Also, further source of alteration is expected through the physical property variation where these properties depend strongly on the temperature distribution thereby influencing strongly the fluid motion. However, the description of the flow physics is not completed here because one needs to look into the inherent temperature dependence of the ionic species. This contribution comes into the picture via the ionic species transport, typically known as the Soret effect. The movement of the ionic species in a thermal gradient is a response subject to the imposed temperature gradient. This effect is incorporated through the thermo-diffusion term ($n_i D_{Ti} \nabla T$) in the Nernst–Planck equation (the dimensionless form of Nernst–Planck equation is shown by equation (S9) of the supplementary material) where the Soret coefficient ($S_{Ti} = D_{Ti}/D_i = Q_i/k_B T^2$) depends on the heat of transport of ions (Q_i). Here, Q_i is the quantification of the degree of sensitivity of ionic mobility with temperature, i.e. thermophoretic mobility of ions. Now, let us first consider the sole action of the Soret effect on the flow dynamics by assuming the absence of any other pertinent forces. A positive value of Q_i suggests that ions should have a propensity to move towards the cold region from the hot region and as a result a thermoelectric field should be induced in the same direction while role reversal should be observed for negative Q_i. Interestingly, the conventional streaming field arising from the imposed pressure gradient is induced in the reverse direction to the applied pressure gradient, i.e. from the hot region to the cold region. So, the thermal-gradient-induced thermoelectric streaming field (assuming positive value of Q_i) seems to act in the same direction as the pressure-gradient-induced streaming field and intuition tells us that the combined action of these two gradients should result in

Dimensionless parameters	Expression	Physical significance	Typical range of parameters
γ	$\gamma = \Delta T/T_C$	Thermal perturbation parameter	$0 \leqslant \gamma \leqslant 0.1$
C_μ	$C_\mu = -(1/\mu)(\partial\mu/\partial T)T_C$	Relative sensitivity of fluid viscosity with temperature	$10^{-1} \leqslant C_\mu \leqslant 10$
C_ε	$C_\varepsilon = -(1/\varepsilon)(\partial\varepsilon/\partial T)T_C$	Relative sensitivity of fluid electrical permittivity with temperature	$10^{-1} \leqslant C_\varepsilon \leqslant 10$
C_k	$C_k = (1/k)(\partial k/\partial T)T_C$	Relative sensitivity of fluid thermal conductivity with temperature	$C_k = 1$
χ	$\chi = (D_+ - D_-)/(D_+ + D_-)$	Diffusivity difference between ions	$-0.3 \leqslant \chi \leqslant 0$
$\Delta\overline{S}_T$	$\Delta\overline{S}_T = (\overline{S}_{T+} - \overline{S}_{T-})$	Difference in Soret coefficients between ions	$0 \leqslant \Delta\overline{S}_T \leqslant 1$
$-\partial\overline{p}_0/\partial\overline{x}$	$-\partial\overline{p}_0/\partial\overline{x} = (-\partial p_0/\partial x)(h^2/\mu u_c)$	Strength of imposed pressure gradient	$0 \leqslant -\partial\overline{p}_0/\partial\overline{x} \leqslant 10$
$\overline{\kappa}_0$	$\overline{\kappa}_0 = \left(\sqrt{\dfrac{2n_\infty z^2 e^2}{\varepsilon_{ref} k_B T}}\right) h$	Inverse of the EDL thickness (determines degree of confinement)	$1 \leqslant \overline{\kappa}_0 \leqslant 10$
C_D	$C_D = (1/D)(\partial D/\partial T)T_C$	Relative sensitivity of diffusivity of ions with temperature	$0 \leqslant C_D \leqslant 5$
C_ζ	$C_\zeta = (1/\zeta_{ref})(\partial\zeta/\partial T)T_C$	Relative sensitivity of zeta potential with temperature	$0 \leqslant C_\zeta \leqslant 4$
De (Deborah number)	$De = \lambda_{ref}\kappa_{ref}u_c$	Relative sensitivity of elastic and viscous effects	$0 \leqslant De \leqslant 1$
C_λ	$C_\lambda = -(1/\lambda_R)(\mathrm{d}\lambda_R/\mathrm{d}T)T_C$	Relative sensitivity of fluid relaxation time with temperature	$0.25 \leqslant C_\lambda \leqslant 3$

TABLE 1. The dimensionless parameters, their expressions, physical significance and typical ranges.

an enhancement of the net induced streaming potential. However, the situation does not remain the same if there is a difference in thermophoretic mobilities between the co-ions (here negative ions) and counter-ions (positive ions). The extent of thermophobic behaviour, i.e. the tendency of ions to move away from the hot region, can change depending on the difference in the thermophoretic mobilities ($\Delta\overline{S}_T$) between cations and anions. Increasing $\Delta\overline{S}_T$ indicates higher heat of transport of counter-ions compared to co-ions, so the counter-ions are more likely to move towards the cold region than the co-ions. This leads to a clear axial separation between the ions and gives rise to an accumulation of the counter-ions in the upstream section, i.e. in the cold region. This induces a form of thermoelectric field downstream (because of $\Delta\overline{S}_T$) while another form of it is formed upstream (because of the sole action of the Soret effect). Hence, the net streaming field (due to combined pressure-driven and temperature-gradient-induced flow) depends on the relative strength of these two counteracting thermoelectric fields. For very low value of $\Delta\overline{S}_T$, these two opposing

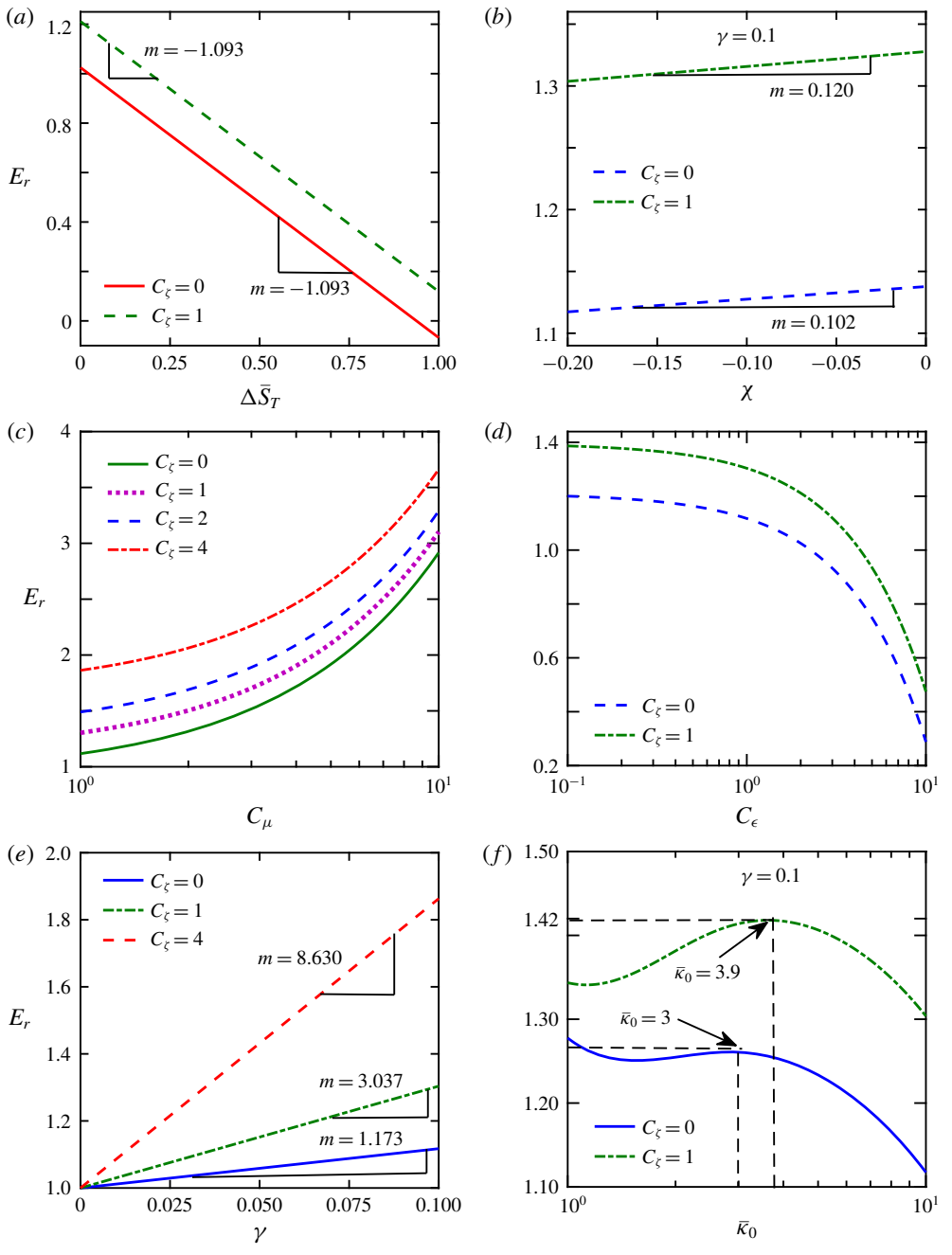

FIGURE 2. Dependence of streaming potential ratio (E_r) on (*a*) $\Delta\bar{S}_T$, (*b*) χ, (*c*) C_μ, (*d*) C_ε, (*e*) γ and (*f*) $\bar{\kappa}_0$.

factors are comparable to each other and the streaming potential ratio (E_r) is close to unity up to $\Delta\bar{S}_T = 0.05$. As one starts increasing $\Delta\bar{S}_T$, the effect of $\Delta\bar{S}_T$-induced streaming field overshadows the temperature-gradient-induced streaming field and net streaming potential ratio experiences a massive reduction. For higher $\Delta\bar{S}_T$, the effect

becomes so pronounced that it completely nullifies the pressure-gradient-induced streaming field (shown by the red solid line in figure 2*a*).

Now, we look into the expression of the bulk number density of ions which reads as $(\partial \ln \overline{n}_i/\partial \overline{x}) = -\overline{S}_{Ti}(\partial\theta/\partial\overline{x})\gamma$ (equation (S11) of the supplementary material, where $\overline{x}$ is the dimensionless axial coordinate, $\overline{x} = x/l$; $\overline{n}_i$ the dimensionless bulk number concentration, $\overline{n}_i = n_i/n_0$; $\overline{S}_{Ti}$ the dimensionless Soret coefficient of ions, $\overline{S}_{Ti} = (D_{Ti}/D_i)T_C$; and θ the dimensionless temperature, $\theta = (T - T_C)/\Delta T_{ref}$), which clearly tells us that the application of the external ΔT in the positive x direction induces an axial concentration gradient of ions in the opposite direction, i.e. from the hot region to the cold region. The concentration gradient $(\partial\overline{n}_i/\partial\overline{x})$ creates a migration of the ions towards the upstream section. Now, we focus our attention towards the definition of the parameter $\chi = (D_+ - D_-)/(D_+ + D_-)$ which is an indicator of the diffusivity difference between the cations and anions. A positive value of χ implies that the diffusivity of cations (here counter-ions) is higher than that of anions which leads to more migration of counter-ions upstream. As a result, there will be an accumulation of counter-ions upstream, while downstream there will be more co-ions. This segregation of ions in different axial locations creates an axial separation between them thus creating a stronger induced streaming field. A negative value of χ means more mobility of anions thereby leading to more accumulation of co-ions in the upstream section resulting in a weaker streaming field. Here we show the variation of streaming potential ratio (E_r) for χ ranging from -0.2 to 0 (figure 2*b*). Here, the value of χ is ion-specific. For typical electrolyte solutions like aqueous KCl, NaCl and LiCl, the value of χ ranges between -0.3 and 0 (approximately) (Zhang *et al.* 2019) and we have chosen the range of χ accordingly when presenting the results.

On closely observing the governing equations involving velocity profile and induced streaming field (equations (S21) and (S26) of the supplementary material), one can understand that the contribution of C_μ comes through the viscous resistance term in the fluid advective motion and the subsequent advective current calculation involved in the electroneutrality condition. Since C_μ indicates the temperature sensitivity of viscosity with temperature, increasing C_μ means viscosity becomes more susceptible to any change in temperature thus resulting in a strong reduction in fluid viscosity. Therefore, the viscous resistance to the flow reduces to a great extent. Thus, the induced streaming field due to migration of ions upon applying a pressure gradient and the streaming field due to migration of ions with induced concentration gradient assist each other (both are induced in the direction from the hot region to the cold region) resulting in significant augmentation in the streaming potential ratio (E_r). Here, increasing C_μ from 1 to 10 results in $\sim$3 times (shown by the green solid line) augmentation of the streaming potential ratio (E_r), as seen in figure 2(*c*).

Now, examining the equation describing the potential distribution (equation (S13) of the supplementary material), it can be observed that unlike the conventional electrokinetic problem, here the EDL thickness (λ_D) no longer remains constant. Instead, the effective EDL thickness (λ_{Deff}) becomes a strong function of temperature and departs significantly from its reference value (of isothermal condition) in the following way: $\overline{\lambda}_{D_{eff}} = \overline{\lambda}_{D_0}\sqrt{\exp\{-\gamma\theta(C_\varepsilon - \overline{S}_{Tavg})\}}$. Keeping other parameters fixed, with increasing C_ε (which is the temperature sensitivity of the electrical permittivity) streaming potential ratio (E_r) decreases sharply by following an exponential thinning behaviour. Since electrical permittivity decreases with temperature, the thickness of the EDL also decreases which results in less penetration of diffuse layer of the EDL to the bulk, so greater is the region of electroneutrality (which means the

region where there is equal number of counter-ions and co-ions). Now, the strength of streaming current involved in the streaming potential estimation depends on this degree of penetration. In the region $10^{-1} \leqslant C_\varepsilon \leqslant 1$, the rate of reduction of E_r with C_ε is not significant: it decreases slightly from 1.2 to 1.1. However, this reduction becomes amplified beyond $C_\varepsilon \sim 1$; E_r decreases sharply and falls to $\sim$0.2 at $C_\varepsilon = 10$ (figure 2*d*).

For fixed value of the factors mentioned above, like $\Delta\overline{S}_T$, χ, C_μ and C_ε, since this analysis is restricted up to order γ, a linear dependence is expected of perturbation parameter on flow field and streaming potential. In figure 2(*e*), C_ζ indicates the relative sensitivity of zeta potential with temperature. For constant zeta potential ($C_\zeta = 0$), E_r is increased up to $\sim$1.12 times as γ varies from 0 to 0.1. However, for temperature-dependent zeta potential, its enhanced sensitivity with temperature results in a significant increase of streaming potential where E_r increases up to $\sim$1.3 and $\sim$1.85 times for $C_\zeta = 1$ and $C_\zeta = 4$, respectively (figure 2*e*).

Now, the degree of confinement is incorporated within the parameter $\overline{\kappa}_0$, i.e. inverse of the thickness of the EDL. The variation of streaming potential ratio (E_r) with $\overline{\kappa}_0$ is shown in figure 2(*f*). Increasing $\overline{\kappa}_0$, on the one hand, increases the region of electroneutrality (ensuring a reduction of streaming current), while on the other hand, the strength of acting electrokinetic forces becomes modulated and net E_r is decided by these two factors. For the case of constant zeta potential (i.e. $C_\zeta = 0$), E_r first decreases with $\overline{\kappa}_0$ up to $\overline{\kappa}_0 = 1.7$, then increases slowly up to $\overline{\kappa}_0 = 3$, beyond which it falls sharply resulting in only $\sim$1.12 times increase of E_r at higher $\overline{\kappa}_0$ ($\overline{\kappa}_0 = 10$). However, the presence of amplified zeta potential (for temperature-dependent zeta potential case, i.e. $C_\zeta = 1$) means role reversal of $\overline{\kappa}_0$ as E_r first increases with $\overline{\kappa}_0$ in the region $1 \leqslant \overline{\kappa}_0 \leqslant 3.9$, beyond which similar decaying behaviour (as seen for $C_\zeta = 0$) with $\overline{\kappa}_0$ is observed (figure 2*f*).

Now we recall the boundary condition involved in evaluating the potential distribution, i.e. where $\overline{\psi} = \psi/\zeta$ is the dimensionless zeta potential $\overline{\psi} = [1 + C_\zeta \gamma\theta]$. Instead of being constant, zeta potential gradually develops in the axial direction. Any alteration in the zeta potential creates a perturbation in the near-wall fluid velocity and affects the adjacent layer of flow through viscous interaction. This axial variation of zeta potential affects the fluid momentum transport by generating a secondary component of flow. Overall, one important conclusion from figure 2 is that as far as the thermoelectric energy conversion is concerned, the inclusion of temperature-dependent zeta potential should be necessary else this could lead to a grossly erroneous estimation of induced streaming potential.

Figure 3 mainly highlights the effect of two parameters, C_ε and $\Delta\overline{S}_T$, on the velocity distribution both in the absence and in the presence of external pressure gradient. In the absence of pressure gradient, the flow physics is solely governed by the external temperature difference and the velocity profile here follows uniform plug-type distribution (evident in both figures 3*a* and 3*c*) which is also typically observed in purely electro-osmotic flows. As one starts introducing pressure gradient ($-\partial\overline{p}_0/\partial\overline{x} = 0.001$), departure from uniformity in flow field is noticeable and at higher strength of pressure gradient ($-\partial\overline{p}_0/\partial\overline{x} = 0.01$), velocity distribution becomes parabolic similar to Poiseuille flow. At higher strength, the effect of pressure gradient becomes so dominant that it dictates the flow physics where the effect of thermal gradient becomes overshadowed. As already discussed, keeping other parameters constant, increasing C_ε results in higher sensitivity of electrical permittivity with temperature which results in attenuation of the EDL thickness thus leading to a reduction in the streaming current and the induced streaming field. So, the strength

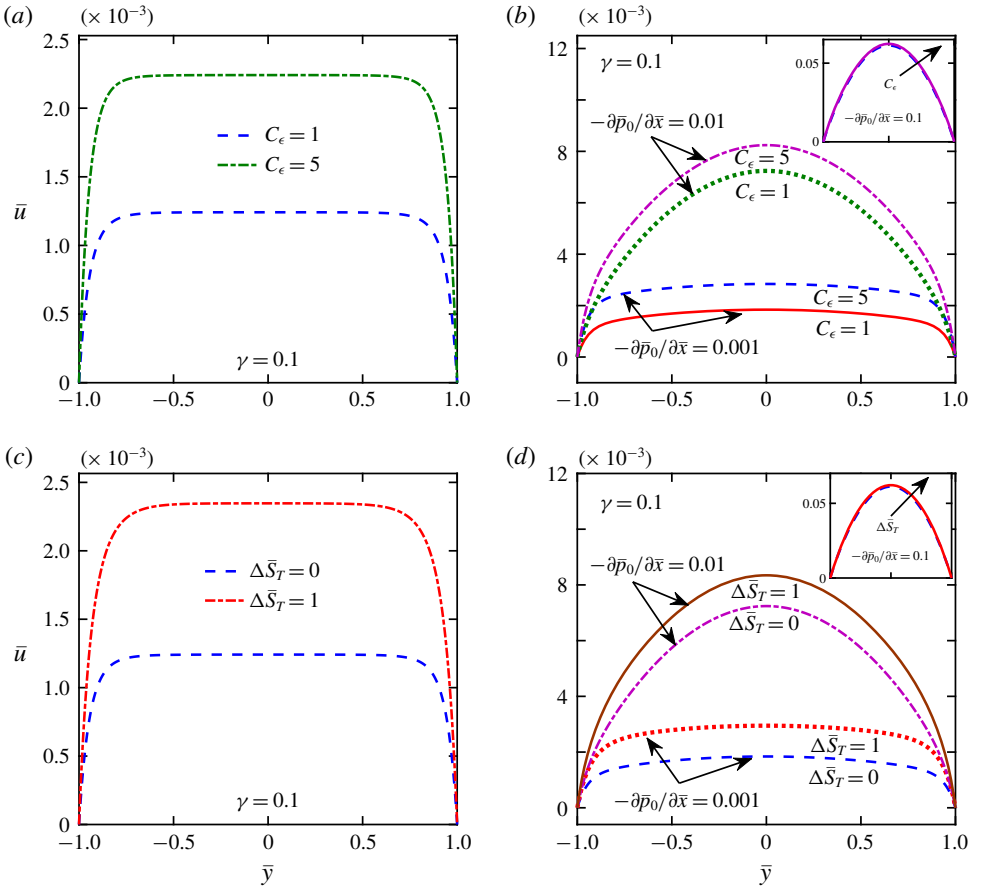

FIGURE 3. Velocity profile in the y direction (a) in the absence and (b) in the presence of pressure gradient for different C_ε. Variation of the same (c) in the absence and (d) in the presence of pressure gradient for different $\Delta\bar{S}_T$ (evaluated at $\bar{x} = 1$).

of streaming-field-driven back electro-osmotic flow also decreases thereby resulting in an enhancement in the magnitude of the net flow velocity. In the absence of pressure gradient, an increment of $\sim$1.8 times can be observed as one increases C_ε from 1 to 5. Now, the rate of increase in velocity magnitude upon increasing C_ε gets damped as one introduces pressure gradient where an increase up to $\sim$1.54 times and $\sim$1.14 times in flow velocity magnitude are observed for $-\partial\bar{p}_0/\partial\bar{x} = 0.001$ and $-\partial\bar{p}_0/\partial\bar{x} = 0.01$, respectively, as seen in figure 3(b). Increasing pressure gradient beyond 0.01 makes it so dominant that the effect of C_ε becomes indistinguishable (inset of figure 3b).

The effect of $\Delta\bar{S}_T$ on the velocity field is shown in figures 3(c) and 3(d) where increasing $\Delta\bar{S}_T$ signifies increasing heat of transport of counter-ions creating enhanced axial separation of ions. The resulting thermoelectric streaming field acts in the opposite direction to that induced due to concentration gradient (which is induced due to external ΔT)-driven migration of ions thus leading to a suppression of the net streaming field and reverse electrokinetic flow. As a result, augmentation up to $\sim$1.9 times in velocity magnitude is seen as $\Delta\bar{S}_T$ varies from 0 to 1. Here also, with

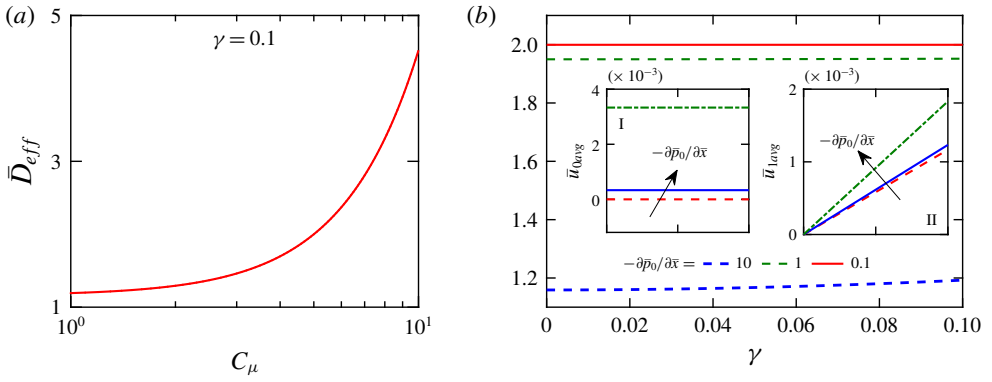

FIGURE 4. (*a*) Dependence of the dispersion coefficient ratio ($\overline{D}_{eff}$) on C_μ. (*b*) Variation of the dispersion coefficient ratio ($\overline{D}_{eff}$) with γ for varying strength of imposed pressure gradient. Insets I and II show the average velocity values of leading order and $O(\gamma)$ with γ for three different values of non-dimensional pressure gradient (0, 10^{-3} and 10^{-2}).

growing pressure gradient, its effect on the flow field starts to become important thus suppressing the effectiveness of $\Delta\overline{S}_T$. As clear from figure 3(*d*), as pressure gradient is increased 10-fold ($-\partial\overline{p}_0/\partial\overline{x} = 0.01$), velocity magnitude with $\Delta\overline{S}_T$ is increased only up to ∼1.15 times (while for $-\partial\overline{p}_0/\partial\overline{x} = 0.001$, this ratio is ∼1.6). Beyond this, the effect of $\Delta\overline{S}_T$ on the flow field becomes inconsequential (evident from the inset).

Figure 4 highlights the dependence of the dispersion coefficient ratio ($\overline{D}_{eff}$) on the parameters involved, where $\overline{D}_{eff}$ is the ratio of the net dispersion resulting from the combined action of two driving forces, pressure gradient and thermal gradient, with respect to that arising from the sole action of pressure gradient. From the definition of hydrodynamic dispersion coefficient (see (2.4)), it is clearly evident that any small change in the flow field results in introduction of higher perturbation in the dispersion coefficient as compared to the net volumetric throughput. This is because the estimation of dispersion coefficient involves parameters like non-dimensional average velocity and plate height, where the plate height further depends on the square of the mean velocity thus showing strong dependence on the flow field. In contrast to Poiseuille flow, in the case of electro-osmotic flow, because of the uniformity in flow field, the main contribution of solute dispersion in the absence of shear-induced dispersion comes from molecular diffusional dispersion thus resulting in lower extent of dispersion. Since pressure-driven flow of electrolyte induces an electro-osmotic flow in the reverse direction, the combined effect of these two results in reduction of the net dispersion coefficient. However, in the presence of an external thermal gradient, the induced thermoelectric streaming field may aid or oppose the pressure-gradient-induced streaming field depending on the different fluidic conditions or parameters as discussed earlier. A typical variation of dispersion coefficient ratio ($\overline{D}_{eff}$) with C_μ is illustrated in figure 4(*a*). Evaluated at $\gamma = 0.1$, $\overline{D}_{eff}$ obeys a linear relationship with C_μ at the initial stages (for $1 \leqslant C_\mu \leqslant 2$), then increases abruptly to experience a pronounced amplification of dispersion coefficient ratio as an increase of ∼4.5 times in $\overline{D}_{eff}$ with C_μ can be seen from figure 4(*a*).

The variation of $\overline{D}_{eff}$ with γ is shown in figure 4(*b*), where γ is the ratio of the imposed temperature difference to the cold-side temperature which determines the degree of thermal perturbation to the flow field. In insets I and II of figure 4(*b*), we

have presented the dimensionless average velocity variations for leading order ($\overline{u}_{0avg}$, which represents the sole effect of pressure gradient) and first-order degree $O(\gamma)$ of perturbations ($\overline{u}_{1avg}$, which shows the effect of thermal perturbation). The red dotted line in inset II shows the dependence of the average velocity for purely thermally (ΔT) driven flow (i.e. $-\partial\overline{p}_0/\partial\overline{x}=0$). In the insets, results are shown for increasing strength of pressure gradient ($-\partial\overline{p}_0/\partial\overline{x}$, dimensionless) starting from 0 to 10^{-2} (three values of $-\partial\overline{p}_0/\partial\overline{x}$ are chosen: 0, 10^{-3} and 10^{-2}). For $O(\gamma)$ average velocity $\overline{u}_{1avg}$, an increase in the slope with increasing pressure gradient can be noticed. However, when one compares insets I and II, one can understand that the rate of enhancement of the average velocity magnitude with increasing $-\partial\overline{p}_0/\partial\overline{x}$ is higher in leading order (i.e. $\overline{u}_{0avg}$) as compared to the increase in $O(\gamma)$ average velocity (i.e. $\overline{u}_{1avg}$). Since the dispersion coefficient is directly related to the square of the average velocity, it is reflected in the variation of $\overline{D}_{eff}$ with γ. With increasing strength of pressure gradient, although the net magnitude of dispersion coefficient becomes lower, its sensitivity with thermal perturbation parameter γ increases and at $-\partial\overline{p}_0/\partial\overline{x}=10$, $\overline{D}_{eff}$ increases from $\sim$1.16 times to $\sim$1.19 times as γ changes from 0 to 0.1 (shown by blue dotted line), while at lower pressure gradient it remains constant at $\overline{D}_{eff}\sim 2$ at $-\partial\overline{p}_0/\partial\overline{x}=0.1$ (shown by red solid line).

Another important parameter influencing the flow physics is the degree of channel confinement ($\overline{\kappa}_0$), depending on which the interacting forces may become predominant or become insignificant. The effect of $\overline{\kappa}_0$ on dispersion coefficient ratio ($\overline{D}_{eff}$) is demonstrated in figure 5. Irrespective of the degree of thermal perturbation (value of γ), here $\overline{D}_{eff}$ decreases gradually with increasing $\overline{\kappa}_0$, and beyond a critical value of $\overline{\kappa}_0$, it reaches a constant value where this magnitude becomes higher with increasing γ with saturation occurring relatively earlier (figure 5*a*). The reduction in the streaming current and resulting streaming potential with increasing C_ε leads to an increase in dispersion coefficient as $\overline{D}_{eff}$ rises to $\sim$1.29 from 1.22 as C_ε is changed from 1 to 10 (evaluated at $\gamma=0.1$, as shown in figure 5*b*). The dependence with $\overline{\kappa}_0$ for varying C_ε is similar to figure 5(*a*) where, after decaying gradually, $\overline{D}_{eff}$ approaches a constant value at higher $\overline{\kappa}_0$ with saturation occurring later at higher γ. Also, at higher γ, the influence of C_ε on dispersion coefficient is greater because of strengthened thermoelectric perturbation. In figure 5(*c*), variation of the same with $\overline{\kappa}_0$ is shown with varying C_μ for two different strengths of pressure gradient. For lower strength ($-\partial\overline{p}_0/\partial\overline{x}=1$), $\overline{D}_{eff}$ first decreases with $\overline{\kappa}_0$ for lower C_μ and approaches a constant value beyond $\overline{\kappa}_0=2.3$, while role reversal is observed for higher C_μ (with saturation occurring later) because of pronounced reduction of flow resistance. For higher strength ($-\partial\overline{p}_0/\partial\overline{x}=10$), the variation of $\overline{D}_{eff}$ with $\overline{\kappa}_0$ remains unaffected for lower C_μ, while at higher C_μ, after increasing gradually with $\overline{\kappa}_0$, $\overline{D}_{eff}$ reaches a constant value of $\sim$4.5 later at $\overline{\kappa}_0=5.2$. Overall, the magnitude of $\overline{D}_{eff}$ always remains much higher compared to unity because of easier actuation of flow owing to lesser viscous resistance. At lower strength of pressure gradient (i.e. $-\partial\overline{p}_0/\partial\overline{x}=1$), the reduction of streaming potential with thermophoretic mobility difference ($\Delta\overline{S}_T$) is reflected through the enhancement of $\overline{D}_{eff}$ with increasing $\Delta\overline{S}_T$ as depicted in figure 5(*d*), although the influence is very weak. At higher strength (shown in the inset of figure 5*d*), trends are similar where the magnitude of $\overline{D}_{eff}$ is reduced from $\sim$2.005 to $\sim$1.97 as seen in figure 5(*d*).

4.2. *Effect of transverse temperature gradient*

Both the cases of axially applied temperature gradient and temperature gradient applied in the transverse direction are of fundamental importance as far as the

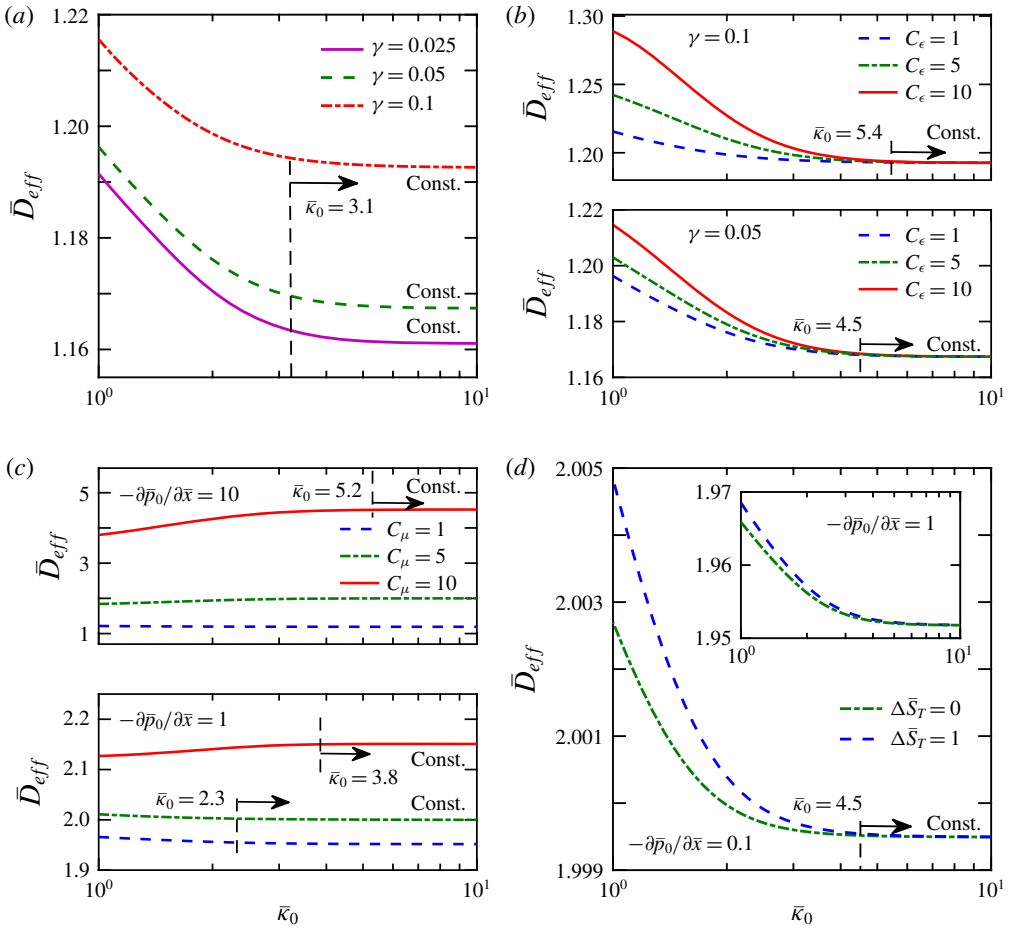

FIGURE 5. Variation of dispersion coefficient ratio with $\bar{\kappa}_0$ for different (*a*) γ, (*b*) C_ε, (*c*) C_μ and (*d*) $\Delta\bar{S}_T$.

hydrodynamic dispersion characteristics are concerned. For the sake of conciseness, we have presented the results for the transverse thermal gradient in § D of the supplementary material.

4.3. *Effect of fluid rheology*

The inclusion of the effect of rheological aspects of fluid on streaming potential is highlighted in figure 6 where the variation of the streaming potential ratio (E_r) with Deborah number (De) is shown in the case of an axially applied thermal gradient. For simplicity of analysis, here we have chosen dilute polymeric solution mixed with electrolyte (aqueous solutions of well-known polymers like polyethylene oxide or polyacrylamide can be taken as examples) as a reference viscoelastic fluid. If the polymer concentration remains below a certain threshold concentration (commonly known as cross-over or overlap concentration), no interaction between the polymer chains can take place and we can assume the solution to belong within the dilute regime (Tirtaatmadja, McKinley & Cooper-White 2006; Del Giudice *et al.* 2015;

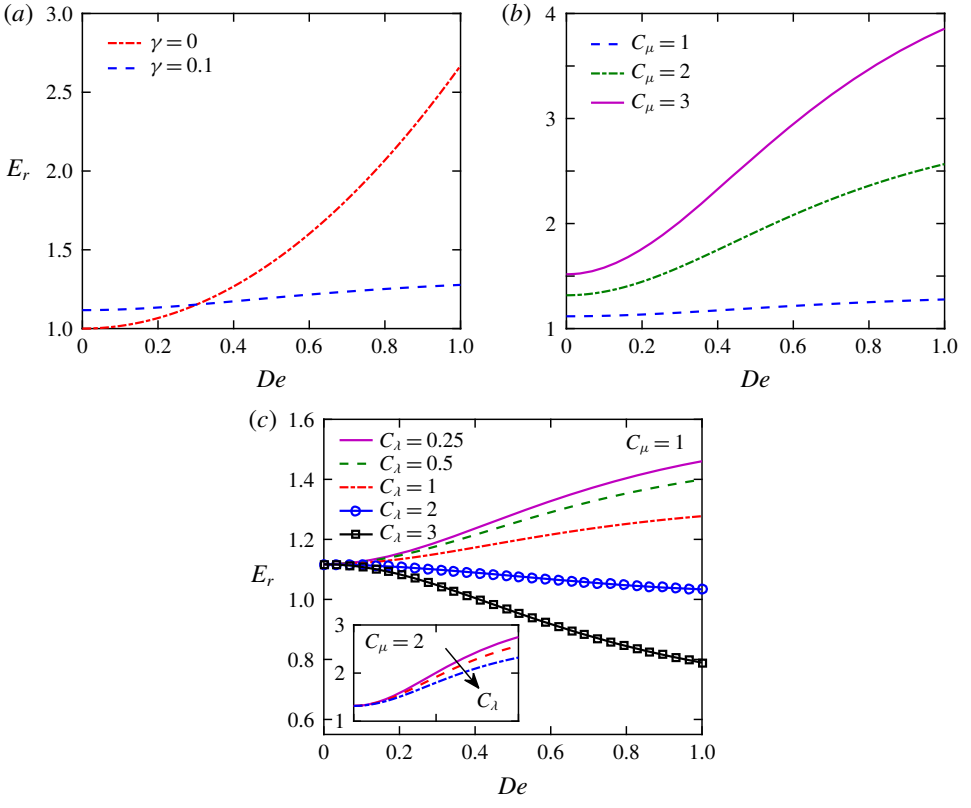

FIGURE 6. Streaming potential ratio (E_r) as a function of Deborah number (De) for different (*a*) γ, (*b*) C_μ and (*c*) C_λ.

Del Giudice, Haward & Shen 2017). For dilute solutions, the imposed driving force creates a disturbance to the polymer chain, in response to which there is an expansion of the polymer chain (Larson 2005). This expansion in turn returns a disturbance to the flow field thus influencing the velocity distribution. Here, it is necessary to highlight the significance of Deborah number (De) which determines the relative strength between elastic and viscous effects. The higher the value of De, the higher is the extent of viscoelasticity, which can be attributed to either increased elasticity of fluid (thus creating more disturbance in the flow field) or attenuated viscous resistance in the flow (because of pronounced shear-thinning effect). For purely pressure-driven flow ($\gamma = 0$, i.e. isothermal condition), elastic behaviour of fluid remains unaffected and increasing De causes a significantly amplified shear-thinning effect which facilitates the fluid advective motion, and therefore streaming potential ratio (E_r) increases up to $\sim$2.7 times as compared to a Newtonian fluid (i.e. $De = 0$). Now, as thermal gradient is imposed, the degree of viscoelasticity gets strongly influenced as fluid viscosity and relaxation time both become strong functions of temperature. Here, it is worth mentioning that in the dilute regime, the relaxation time of a polymeric solution remains independent of the polymer concentration, described by the widely known Zimm relaxation time (λ_z) (Tirtaatmadja *et al.* 2006; Del Giudice *et al.* 2017; Pan *et al.* 2018). Previous experimental studies have reported an inverse relationship of λ_z with temperature which can be approximated by an

exponential thinning behaviour (i.e. in the form of $\lambda_{eff} = \lambda_{ref} \exp[-\omega_4(T - T_{ref})]$) (Pan *et al.* 2018). It is important to mention that although λ_z has been widely used in the rheological characterization of polymeric fluids, some experimental studies have reported that, even for dilute solutions, fluid relaxation time can vary with the polymer concentration (Tirtaatmadja *et al.* 2006). The effective relaxation time (λ_{eff}) can be up to one order of magnitude higher than the Zimm relaxation time depending on polymer concentration. Here, we have chosen the Zimm relaxation time to represent the results for viscoelastic fluids, while the variation of relaxation time with polymer concentration and its consequences for streaming potential and dispersion coefficient are highlighted in § E1 of the supplementary material.

As evident from the governing equation of viscoelastic fluids (equation (S56) of the supplementary material), the net effect of viscoelasticity on streaming potential depends on the relative sensitivity of viscosity (C_μ) and relaxation time (C_λ) of fluid with temperature. For a fixed value of C_μ and C_λ, introducing thermal gradient ($\gamma = 0.1$) results a reduction in the net streaming potential with De where an increase of $\sim$1.27 times in E_r is observed as opposed to $\sim$2.7 times increase for $\gamma = 0$ (figure 6*a*). Interestingly, a cross-over at $De = 0.3$ takes place between the graphs of $\gamma = 0$ and $\gamma = 0.1$. Below this critical De, the magnitude of the streaming potential is higher for combined temperature-gradient- and pressure-driven flow, and beyond De = 0.3, it falls below the streaming potential in isothermal condition in which case the strongly pronounced shear-thinning effect with increasing De dictates the flow physics creating faster rise in streaming potential. Now, at lower C_μ (denoting lower temperature sensitivity of fluid viscosity), the two previously mentioned counteracting factors are of comparable magnitude resulting in a slight increase in E_r (from 1.12 times to 1.28 times) as De varies from 0 to 1, seen in figure 6(*b*). With increasing C_μ, its effect starts to become dominant over C_λ and E_r undergoes significant enhancement up to $\sim$3.86 times (at $C_\mu = 3$) compared to a Newtonian fluid. Similarly, increasing C_λ from 0.25 leads to faster reduction in fluid relaxation time denoting elevated elasticity-mediated disturbance to the axial separation between ions thus lowering the net streaming potential. As evident from figure 6(*c*), E_r decreases from 1.46 to 0.79 as C_λ is increased from 0.25 to 3. Beyond $C_\lambda = 1$, E_r starts to fall with De (from its reference value $\sim$1.12) and becomes less than unity at higher De. This tells us that if C_λ is high (i.e. rapid reduction of fluid relaxation time with temperature), employing a Newtonian fluid is more advantageous than employing a viscoelastic fluid as far as streaming potential generation is concerned. Now, as shown in the inset of figure 6(*c*), the influence of C_λ on streaming potential gets damped at higher C_μ ($C_\mu = 2$) where E_r reduces at a lower rate from 2.75 times to 2.3 times (with respect to a Newtonian fluid) with increasing C_λ.

This section has reached its culmination where the dependence of the dispersion coefficient ratio ($\overline{D}_{eff}$) on Deborah number (De) is shown in figure 7 for two crucial parameters C_μ and C_λ. Similar to the variation of E_r, $\overline{D}_{eff}$ is also highly sensitive to the variation in fluid viscosity and relaxation time. Looking into the constitutive form of a viscoelastic fluid one can realize that the inherent nonlinearity in stress-tensor terms becomes amplified with increasing C_μ. Physically, the impact of physical property alteration is reflected more in viscoelastic fluids compared to Newtonian fluids and, accordingly, $\overline{D}_{eff}$ increases up to 1.9 times at higher C_μ (at $C_\mu = 3$). Also, changing C_λ can result in significant alteration in the dispersion coefficient where $\overline{D}_{eff}$ exhibits an inverse dependence on De at higher C_λ, as observed in figure 7(*b*). Overall, $\overline{D}_{eff}$ undergoes a reduction from 1.53 to 1.1 as C_λ is increased from 0.25 to 3.

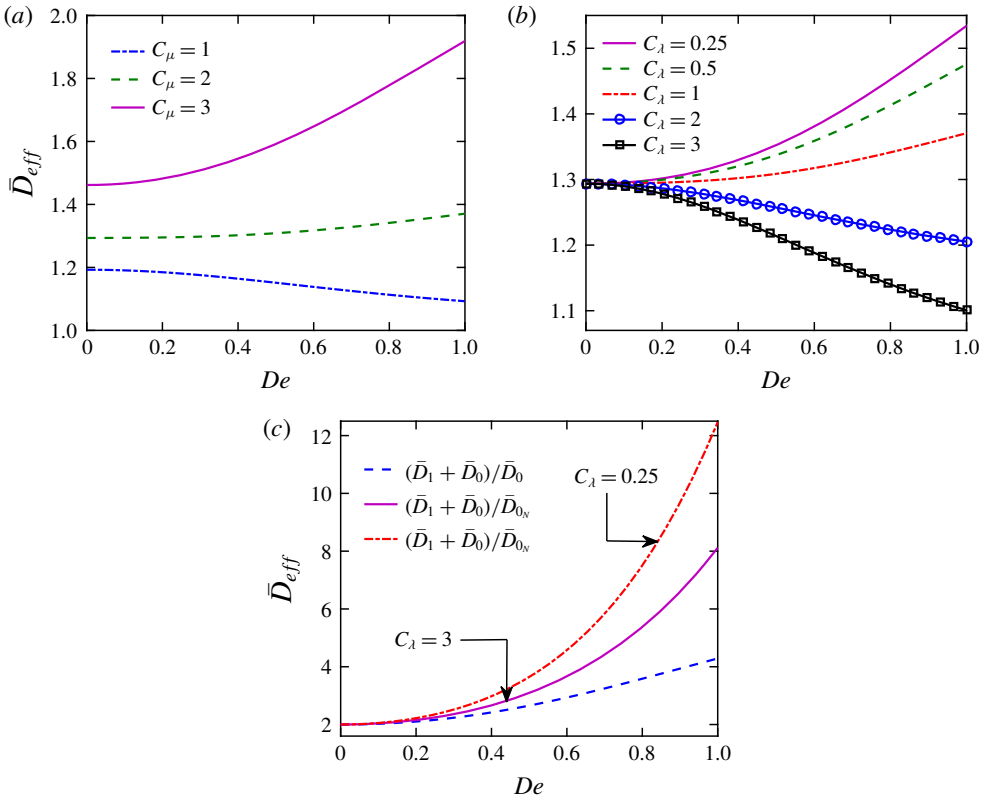

FIGURE 7. Variation of dispersion coefficient ratio ($\overline{D}_{eff}$) with Deborah number (De) for (a) different C_μ and (b) different C_λ. (c) Variation of $\overline{D}_{eff}$ for specific combinations of C_μ and C_λ.

If one considers the volumetric flow rate variation for the case of viscoelastic fluid (this is presented in § E2 of the supplementary material), it is clearly evident that increasing C_μ and decreasing C_λ turn out to be favourable as far as the enhancement of dispersion is concerned. When we combine these two factors, under strong thermal perturbation (at $\gamma = 0.1$), the variation of $\overline{D}_{eff}$ with De experiences massive augmentation. The dotted blue line represents the ratio of relative increase of $\overline{D}_{eff}$ in viscoelastic fluid for combined pressure-gradient and thermal-gradient-driven flow as compared to that for a purely pressure-driven flow where $\overline{D}_{eff}$ is increased up to ∼4.3 times (figure 7*c*) evaluated at $C_\mu = 5$, $C_\lambda = 0.25$. The red dash-dotted line expresses the ratio of the net dispersion coefficient in viscoelastic fluid to that compared to the solely pressure-driven flow of a Newtonian fluid where it augments further up to ∼12.5 times as De is varied from 0 to 1. Keeping in mind its applicability under actual experimental conditions, we now focus on the physically relevant values of C_μ and C_λ. As reported in the literature, the relative change of fluid viscosity with temperature $-(1/\mu)(\partial\mu/\partial T)$ for electrolyte solutions is approximately 15×10^{-3} K^{-1} (Dietzel & Hardt 2017) which can be used in the expression of $\overline{\mu} = \mu/\mu_{ref} = \exp(-\gamma C_\mu \theta)$, where the value of C_μ turns out to be close to 5. Also the reduction of fluid relaxation time with temperature can be correlated in a similar fashion ($\overline{\lambda} = \lambda_{eff}/\lambda_{ref} = \exp(-\gamma C_\lambda \theta)$) where the value of C_λ is chosen as

3 (the reason behind this particular combination of parameters is discussed in § E2 of the supplementary material). For $C_\mu = 5$, $C_\lambda = 3$, $\overline{D}_{eff}$ is increased up to ∼8.1 times as compared to a Newtonian fluid. Therefore, we conclude that, employing this combination of parameters under the combinatorial effect of external pressure gradient and temperature difference, it is indeed practically possible to achieve an enhancement of up to one order of magnitude (approximately) in the dispersion coefficient. For completeness of the present analysis, the results for transverse thermal gradient are presented in § E3 of the supplementary material.

5. Experimental perspective

A practical experimental set-up can be designed on the basis of the presented theoretical framework. We here discuss an outline of the same. For this purpose, the first step should be microchannel fabrication for which the standard photolithography protocol followed by soft lithography technique can be employed (Raj, Dasgupta & Chakraborty 2017). Typical dimensions of the microchannel can be: width ∼100 μm, height $(h) \sim 50$ μm and length $(l) \sim 5$ cm.

At the two ends of the microchannel, two reservoirs can be made and the microchannel needs to be filled with the electrolyte solution (0.1 to 1 mM aqueous NaCl or aqueous KCl solution can be chosen as an example). The dimensions of the reservoirs should be large enough such that entrance and exit losses can be avoided. It also needs to be ensured that the fluid level at the two reservoirs is balanced perfectly such that no flow can take place by virtue of pressure head. Platinum electrodes should be immersed fully within the fluids in order to ensure proper electrical connectivity. In order to generate the temperature gradient, a strip heater can be employed which is usually connected to a voltage source meter. For the measurement of temperature at both ends, thermocouples along with data acquisition system need to be connected. To apply the pressure gradient, a syringe pump can be used along with a pressure sensor for continuously monitoring the pressure drop. The next step is to measure the induced streaming potential under the combined action of imposed pressure gradient and temperature gradient for which a voltmeter needs to be connected in parallel with the electrode. The higher end of the voltmeter probe needs to be connected to the downstream electrode with the lower end connected with the upstream electrode (Van Der Heyden *et al.* 2005, 2007; Morikawa *et al.* 2010; Das *et al.* 2018).

The final step is the measurement of the hydrodynamic dispersion coefficient for which a plug of dye such as a dilute solution of fluorescein can be prepared first and then it needs to be transported by the combined pressure-driven and temperature-gradient-induced flow of the electrolyte solution. Then the position of the plug along the channel needs to be determined. For a fixed dimension of the channel and fixed flow condition, this measurement needs to be done several times at different locations along the channel. For the recording of the fluorescence intensity, a CCD camera coupled to a microscope can be used along with a mercury lamp (with a specific filter for fluorescein). Recorded data will consist of fluorescence intensities at two different positions falling under the same time scale of observation. The post-processing of the fluorescence images can be done using standard image processing software or by developing an in-house code where the average fluorescence intensity in each position needs to be calculated. Once this intensity is known as a function of time, the mean axial flow velocity (u_{avg}) can then be obtained as $u_{avg} = (x_2 - x_1)/(t_{max\,2} - t_{max\,1})$ (Bontoux *et al.* 2006), with $t_{max\,i}$ indicating the time

required for the intensity to reach its maximum at position i. When the solute equilibrates in the transverse direction after a sufficiently long time passed, the concentration distribution can be given by (Bontoux *et al.* 2006)

$$c = \frac{1}{\sqrt{4\pi D_{eff} t}} \exp\left(-\frac{(x - u_{avg} t)^2}{4 D_{eff} t}\right), \tag{5.1}$$

where D_{eff} denotes the effective dispersion coefficient. In the long-time regime, the position x can be written as $x = u_{avg} t_{max}$ and (5.1) can be rewritten as (Bontoux *et al.* 2006)

$$c = \frac{1}{\sqrt{4\pi D_{eff} t_{max}}} \exp\left(-\frac{{u_{avg}}^2 (t_{max} - t)^2}{4 D_{eff} t_{max}}\right). \tag{5.2}$$

Now, considering the intensity variation in terms of concentration and then fitting the concentration profile in a Gaussian distribution, using the values of its fitting parameters one can determine the dispersion coefficient using a procedure similar to that discussed in Bontoux *et al.* (2006).

One key factor for the experiments is the inclusion of a non-Newtonian fluid. For this purpose, dilute aqueous polymeric solutions such as polyethylene oxide or polyacrylamide can be mixed with the electrolyte solution and then stirred for 24 h (Huang *et al.* 2016; Mukherjee *et al.* 2017*a*). In this context, it is important to mention that the polymer concentration should remain in the dilute regime, i.e. below the threshold concentration c^* (also known as overlap or cross-over concentration) above which it would be difficult to drive the flow because of the strongly enhanced viscous resistance. When the concentration undergoes a transition from the dilute to the semi-dilute regime, both its elastic behaviour (i.e. fluid relaxation time) and viscosity increase with concentration. However, the rate of increase in viscosity is higher as compared to the increase in the fluid relaxation time (Del Giudice *et al.* 2015). Therefore, it will be judicious to operate within the dilute regime where the shear-thinning behaviour of the polymer can be beneficial in driving the fluid because of less viscous resistance compared to the case of a Newtonian fluid.

In previous years, experimental studies of hydrodynamic dispersion were performed usually for pressure-driven flow (Bontoux *et al.* 2006; Ling *et al.* 2018), while studies of non-isothermal electrokinetic flow mainly focused on the Joule heating effect and its consequences for the resulting flow dynamics (Xuan *et al.* 2004; Venditti *et al.* 2006; Xuan 2008). To the best of our knowledge, no such experimental study has been reported for the case of hydrodynamic dispersion in non-isothermal electrokinetic flow. In this scenario, we believe that this present outline can be implemented practically to set up an experimental analysis, while the presented theoretical model provides the relevant parameters and flow conditions with an objective of achieving augmented dispersion by optimizing the relevant physical space.

6. Conclusions

We have considered thermally modulated electrokinetic transport to realize significant enhancement in solute dispersion of a complex fluid through a microfluidic channel. Although several techniques in the past have been deployed towards modulating the uniform velocity profile of electrically actuated flows, improved hydrodynamic dispersion still remains unexplored. In this context, the present study shows that combining the interplay between thermal and electrical effects coupled

with fluid rheology, one can achieve up to one order of magnitude enhancement of dispersion coefficient in a pressure-driven flow of an electrolyte. This is mediated by breaking the equilibrium of the charge distribution within the EDL with imposed thermal gradient, subsequent modulation in thermo-physical properties and eventual alterations in the fluid motion. We believe that such complex coupling between thermal, electrical, hydrodynamic and rheological parameters in small scales can be exploited not only to benefit the design of thermally actuated microfluidic and bio-microfluidic devices demanding improved hydrodynamic dispersion but also can act as a basis for solving several thermal and fluidic problems (Sarkar *et al.* 2002; Dua & Chakraborty 2005; Chakraborty 2007; Chakraborty & Durst 2007; Rana, Chakraborty & Som 2014; Bandopadhyay *et al.* 2016).

Acknowledgement

S.C. acknowledges the Department of Science and Technology, Government of India, for Sir J. C. Bose National Fellowship.

Declaration of interests

The authors declare no conflicts of interest.

Supplementary material

Supplementary material is available at https://doi.org/10.1017/jfm.2020.369.

REFERENCES

AFONSO, A. M., ALVES, M. A. & PINHO, F. T. 2009 Analytical solution of mixed electro-osmotic/pressure driven flows of viscoelastic fluids in microchannels. *J. Non-Newtonian Fluid Mech.* **159** (1–3), 50–63.

AFONSO, A. M., ALVES, M. A. & PINHO, F. T. 2013 Analytical solution of two-fluid electro-osmotic flows of viscoelastic fluids. *J. Colloid Interface Sci.* **395** (1), 277–286.

AJDARI, A. 1995 Electro-osmosis on inhomogeneously charged surfaces. *Phys. Rev. Lett.* **75** (4), 755.

AJDARI, A. 1996 Generation of transverse fluid currents and forces by an electric field: electro-osmosis on charge-modulated and undulated surfaces. *Phys. Rev.* E **53** (5), 4996–5005.

AJDARI, A., BONTOUX, N. & STONE, H. A. 2006 Hydrodynamic dispersion in shallow microchannels: the effect of cross-sectional shape. *Analyt. Chem.* **78** (2), 387–392.

ANDERSON, P. D., GALAKTIONOV, O. S., PETERS, G. W. M., VAN DE VOSSE, F. N. & MEIJER, H. E. H. 2000 Mixing of non-Newtonian fluids in time-periodic cavity flows. *J. Non-Newtonian Fluid Mech.* **93** (2–3), 277–286.

ARCOS, J. C., MÉNDEZ, F., BAUTISTA, E. G. & BAUTISTA, O. 2018 Dispersion coefficient in an electro-osmotic flow of a viscoelastic fluid through a microchannel with a slowly varying wall zeta potential. *J. Fluid Mech.* **839**, 348–386.

ARIS, R. 1956 On the dispersion of a solute in a fluid flowing through a tube. *Proc. R. Soc. Lond.* A **235** (1200), 67–77.

ARIS, R. 1959 On the dispersion of a solute by diffusion, convection, and exchange between phases. *Proc. R. Soc. Lond.* A **252** (1271), 538–550.

BANDOPADHYAY, A. & CHAKRABORTY, S. 2011 Steric-effect induced alterations in streaming potential and energy transfer efficiency of non-Newtonian fluids in narrow confinements. *Langmuir* **27** (19), 12243–12252.

BANDOPADHYAY, A. & CHAKRABORTY, S. 2012 Giant augmentations in electro-hydro-dynamic energy conversion efficiencies of nanofluidic devices using viscoelastic fluids. *Appl. Phys. Lett.* **101** (4), 043905.

BANDOPADHYAY, A., MANDAL, S., KISHORE, N. K. & CHAKRABORTY, S. 2016 Uniform electric-field-induced lateral migration of a sedimenting drop. *J. Fluid Mech.* **792**, 553–589.

BARRAGÁN, V. M. & KJELSTRUP, S. 2017 Thermo-osmosis in membrane systems: a review. *J. Non-Equilib. Thermodyn.* **42** (3), 217–236.

BARTON, N. G. 1983 On the method of moments for solute dispersion. *J. Fluid Mech.* **126**, 205–218.

BAUTISTA, O., SÁNCHEZ, S., ARCOS, J. C. & MÉNDEZ, F. 2013 Lubrication theory for electro-osmotic flow in a slit microchannel with the Phan-Thien and Tanner model. *J. Fluid Mech.* **722**, 496–532.

BECKER, H. & GÄRTNER, C. 2000 Polymer microfabrication methods for microfluidic analytical applications. *Electrophoresis* **21** (1), 12–26.

BERLI, C. L. A. 2010 Electrokinetic energy conversion in microchannels using polymer solutions. *J. Colloid Interface Sci.* **349** (1), 446–448.

BERLI, C. L. A. & OLIVARES, M. L. 2008 Electrokinetic flow of non-Newtonian fluids in microchannels. *J. Colloid Interface Sci.* **320** (2), 582–589.

BONTOUX, N., PEPIN, A., CHEN, Y., AJDARI, A. & STONE, H. A. 2006 Experimental characterization of hydrodynamic dispersion in shallow microchannels. *Lab on a Chip* **6** (7), 930–935.

BRASK, A., KUTTER, J. P. & BRUUS, H. 2005 Long-term stable electroosmotic pump with ion exchange membranes. *Lab on a Chip* **5** (7), 730–738.

BRUST, M., SCHAEFER, C., DOERR, R. & WAGNER, C. 2013 Rheology of human blood plasma: viscoelastic versus Newtonian behavior. *Phys. Rev. Lett.* **110** (7), 078305.

CHAKRABORTY, S. 2006 Analytical solutions of Nusselt number for thermally fully developed flow in microtubes under a combined action of electroosmotic forces and imposed pressure gradients. *Intl J. Heat Mass Transfer* **49** (3–4), 810–813.

CHAKRABORTY, S. 2007 Towards a generalized representation of surface effects on pressure-driven liquid flow in microchannels. *Appl. Phys. Lett.* **90** (3), 034108.

CHAKRABORTY, N. & CHAKRABORTY, S. 2007 Modelling of turbulent molten pool convection in laser welding of a copper–nickel dissimilar couple. *Intl J. Heat Mass Transfer* **50** (9–10), 1805–1822.

CHAKRABORTY, S. & DURST, F. 2007 Derivations of extended Navier–Stokes equations from upscaled molecular transport considerations for compressible ideal gas flows: towards extended constitutive forms. *Phys. Fluids* **19** (8), 088104.

CHAKRABORTY, S. & PADHY, S. 2008 Anomalous electrical conductivity of nanoscale colloidal suspensions. *ACS Nano* **2** (10), 2029–2036.

CHAKRABORTY, S. & SRIVASTAVA, A. K. 2007 Generalized model for time periodic electroosmotic flows with overlapping electrical double layers. *Langmuir* **23** (24), 12421–12428.

CHANG, C. C. & YANG, R. J. 2008 Chaotic mixing in a microchannel utilizing periodically switching electro-osmotic recirculating rolls. *Phys. Rev.* E **77** (5), 056311.

CHATWIN, P. C. 1970 The approach to normality of the concentration distribution of a solute in a solvent flowing along a straight pipe. *J. Fluid Mech.* **43** (2), 321–352.

CHATWIN, P. C. 1975 On the longitudinal dispersion of passive contaminant in oscillatory flows in tubes. *J. Fluid Mech.* **71** (3), 513–527.

CHATWIN, P. C. & SULLIVAN, P. J. 1982 The effect of aspect ratio on longitudinal diffusivity in rectangular channels. *J. Fluid Mech.* **120**, 347–358.

CHEN, C. H., LIN, H., LELE, S. K. & SANTIAGO, J. G. 2005 Convective and absolute electrokinetic instability with conductivity gradients. *J. Fluid Mech.* **524**, 263–303.

CHU, H. C. W., GAROFF, S., PRZYBYCIEN, T. M., TILTON, R. D. & KHAIR, A. S. 2019 Dispersion in steady and time-oscillatory two-dimensional flows through a parallel-plate channel. *Phys. Fluids* **31** (2), 022007.

COELHO, P. M., ALVES, M. A. & PINHO, F. T. 2012 Forced convection in electro-osmotic/Poiseuille micro-channel flows of viscoelastic fluids: fully developed flow with imposed wall heat flux. *Microfluid. Nanofluid.* **12** (1–4), 431–449.

DAS, S. & CHAKRABORTY, S. 2006 Analytical solutions for velocity, temperature and concentration distribution in electroosmotic microchannel flows of a non-Newtonian bio-fluid. *Anal. Chim. Acta* **559** (1), 15–24.

DAS, S. & CHAKRABORTY, S. 2007 Transverse electrodes for improved DNA hybridization in microchannels. *AIChE J.* **53** (5), 1086–1099.

DAS, S. & CHAKRABORTY, S. 2010 Effect of conductivity variations within the electric double layer on the streaming potential estimation in narrow fluidic confinements. *Langmuir* **26** (13), 11589–11596.

DAS, S., DAS, T. & CHAKRABORTY, S. 2006 Analytical solutions for the rate of DNA hybridization in a microchannel in the presence of pressure-driven and electroosmotic flows. *Sensors Actuators* B **114** (2), 957–963.

DAS, S. P., CHAKRABORTY, S. & DUTTA, P. 2004 Studies on thermal stratification phenomenon in LH_2 storage vessel. *Heat Transfer Engng* **25** (4), 54–66.

DAS, S. S., KAR, S., ANWAR, T., SAHA, P. & CHAKRABORTY, S. 2018 Hydroelectric power plant on a paper strip. *Lab on a Chip* **18** (11), 1560–1568.

DATTA, S. & GHOSAL, S. 2008 Dispersion due to wall interactions in microfluidic separation systems. *Phys. Fluids* **20** (1), 012103.

DE LOUBENS, C., MAGNIN, A., DOYENNETTE, M., TRÉLÉA, I. C. & SOUCHON, I. 2011 A biomechanical model of swallowing for understanding the influence of saliva and food bolus viscosity on flavor release. *J. Theor. Biol.* **280** (1), 180–188.

DEL GIUDICE, F., DAVINO, G., GRECO, F., DE SANTO, I., NETTI, P. A. & MAFFETTONE, P. L. 2015 Rheometry-on-a-chip: measuring the relaxation time of a viscoelastic liquid through particle migration in microchannel flows. *Lab on a Chip* **15** (3), 783–792.

DEL GIUDICE, F., HAWARD, S. J. & SHEN, A. Q. 2017 Relaxation time of dilute polymer solutions: a microfluidic approach. *J. Rheol.* **61** (2), 327–337.

DEY, R., CHAKRABORTY, D. & CHAKRABORTY, S. 2011 Analytical solution for thermally fully developed combined electroosmotic and pressure-driven flows in narrow confinements with thick electrical double layers. *J. Heat Transfer* **133** (2), 024503.

DIETZEL, M. & HARDT, S. 2016 Thermoelectricity in confined liquid electrolytes. *Phys. Rev. Lett.* **116** (22), 225901.

DIETZEL, M. & HARDT, S. 2017 Flow and streaming potential of an electrolyte in a channel with an axial temperature gradient. *J. Fluid Mech.* **813**, 1060–1111.

DUA, R. & CHAKRABORTY, S. 2005 A novel modeling and simulation technique of photo-thermal interactions between lasers and living biological tissues undergoing multiple changes in phase. *Comput. Biol. Med.* **35** (5), 447–462.

DUTTA, D. 2008 Electrokinetic transport of charged samples through rectangular channels with small zeta potentials. *Analyt. Chem.* **80** (12), 4723–4730.

FAM, H., BRYANT, J. T. & KONTOPOULOU, M. 2007 Rheological properties of synovial fluids. *Biorheology* **44** (2), 59–74.

FERRÁS, L. L., AFONSO, A. M., ALVES, M. A., NÓBREGA, J. M. & PINHO, F. T. 2016 Electro-osmotic and pressure-driven flow of viscoelastic fluids in microchannels: analytical and semi-analytical solutions. *Phys. Fluids* **28** (9), 93102.

GAO, Y., WONG, T. N., YANG, C. & OOI, K. T. 2005 Two-fluid electroosmotic flow in microchannels. *J. Colloid Interface Sci.* **284** (1), 306–314.

GARAI, A. & CHAKRABORTY, S. 2009 Micro-scale thermo-fluidic transport in two immiscible liquid layers subject to combined electroosmotic and pressure-driven transport. *Intl J. Heat Mass Transfer* **52** (11–12), 2660–2666.

GARCIA, A. L., ISTA, L. K., PETSEV, D. N. & LÓPEZ, G. P. 2005 Electrokinetic molecular separation in nanoscale fluidic channels. *Lab on a Chip* **5** (11), 1271–1276.

GAŠ, B., ŠTĚDRÝ, M. & KENNDLER, E. 1997 Peak broadening in capillary zone electrophoresis. *Electrophoresis* **18** (12–13), 2123–2133.

GHATAK, A. & CHAKRABORTY, S. 2007 Effect of external irreversibilities and variable thermal properties of working fluids on thermal performance of a Dual internal combustion engine cycle. *J. Mech. Energy* **58** (1), 1–12.

GHONGE, T., CHAKRABORTY, J., DEY, R. & CHAKRABORTY, S. 2013 Electrohydrodynamics within the electrical double layer in the presence of finite temperature gradients. *Phys. Rev.* E **88** (5), 53020.

GHOSAL, S. 2002 Lubrication theory for electro-osmotic flow in a microfluidic channel of slowly varying cross-section and wall charge. *J. Fluid Mech.* **459**, 103–128.

GHOSAL, S. 2004 Fluid mechanics of electroosmotic flow and its effect on band broadening in capillary electrophoresis. *Electrophoresis* **25** (2), 214–228.

GHOSAL, S. 2006 Electrokinetic flow and dispersion in capillary electrophoresis. *Annu. Rev. Fluid Mech.* **38** (1), 309–338.

GHOSAL, S. & CHEN, Z. 2012 Electromigration dispersion in a capillary in the presence of electro-osmotic flow. *J. Fluid Mech.* **697**, 436–454.

GHOSH, U. & CHAKRABORTY, S. 2012 Patterned-wettability-induced alteration of electro-osmosis over charge-modulated surfaces in narrow confinements. *Phys. Rev.* E **85** (4), 046304.

GHOSH, U. & CHAKRABORTY, S. 2015 Electroosmosis of viscoelastic fluids over charge modulated surfaces in narrow confinements. *Phys. Fluids* **27** (6), 62004.

GHOSH, U., CHAUDHURY, K. & CHAKRABORTY, S. 2016 Electroosmosis over non-uniformly charged surfaces: modified Smoluchowski slip velocity for second-order fluids. *J. Fluid Mech.* **809**, 664–690.

GHOSH, U., MANDAL, S. & CHAKRABORTY, S. 2017 Electroosmosis over charge-modulated surfaces with finite electrical double layer thicknesses: asymptotic and numerical investigations. *Phys. Rev. Fluids* **2** (6), 1–29.

GLASGOW, I., BATTON, J. & AUBRY, N. 2004 Electroosmotic mixing in microchannels. *Lab on a Chip* **4** (6), 558–562.

GOSWAMI, P., CHAKRABORTY, J., BANDOPADHYAY, A. & CHAKRABORTY, S. 2015 Electrokinetically modulated peristaltic transport of power-law fluids. *Microvasc. Res.* **103**, 41–54.

HAEBERLE, S. & ZENGERLE, R. 2007 Microfluidic platforms for lab-on-a-chip applications. *Lab on a Chip* **7** (9), 1094–1110.

HOSHYARGAR, V., TALEBI, M., ASHRAFIZADEH, S. N. & SADEGHI, A. 2018 Hydrodynamic dispersion by electroosmotic flow of viscoelastic fluids within a slit microchannel. *Microfluid. Nanofluid.* **22** (1), 4.

HUANG, K.-D. & YANG, R.-J. 2006 Numerical modeling of the Joule heating effect on electrokinetic flow focusing. *Electrophoresis* **27** (10), 1957–1966.

HUANG, Y., CHEN, J., WONG, T. & LIOW, J. L. 2016 Experimental and theoretical investigations of non-Newtonian electro-osmotic driven flow in rectangular microchannels. *Soft Matt.* **12** (29), 6206–6213.

HUNTER, R. J. 1981 *Zeta Potential in Colloid Science*. Academic Press.

JANSONS, K. M. 2006 On Taylor dispersion in oscillatory channel flows. *Proc. R. Soc. Lond.* A **462** (2076), 3501–3509.

JOKINEN, M., MANZANARES, J. A., KONTTURI, K. & MURTOMÄKI, L. 2016 Thermal potential of ion-exchange membranes and its application to thermoelectric power generation. *J. Membr. Sci.* **499**, 234–244.

KARNIADAKIS, G., BESKOK, A. & ALURU, N. 2005 *Microflows and Nanoflows: Fundamentals and Simulation*. Springer.

LARSON, R. G. 2005 The rheology of dilute solutions of flexible polymers: progress and problems. *J. Rheol.* **49** (1), 1–70.

LEVINE, S., MARRIOTT, J. R., NEALE, G. & EPSTEIN, N. 1975 Theory of electrokinetic flow in fine cylindrical capillaries at high zeta-potentials. *J. Colloid Interface Sci.* **52** (1), 136–149.

LI, H., WONG, T. N. & NGUYEN, N. T. 2009 Electroosmotic control of width and position of liquid streams in hydrodynamic focusing. *Microfluid. Nanofluid.* **7** (4), 489–497.

LI, H., WONG, T. N. & NGUYEN, N. T. 2011 Microfluidic switch based on combined effect of hydrodynamics and electroosmosis. *Microfluid. Nanofluid.* **10** (5), 965–976.

LI, L. & WANG, Q. 2018 Thermoelectricity in heterogeneous nanofluidic channels. *Small* **14** (21), 1800369.

LING, B., OOSTROM, M., TARTAKOVSKY, A. M. & BATTIATO, I. 2018 Hydrodynamic dispersion in thin channels with micro-structured porous walls. *Phys. Fluids* **30** (7), 076601.

MANDAL, S., GHOSH, U., BANDOPADHYAY, A. & CHAKRABORTY, S. 2015 Electro-osmosis of superimposed fluids in the presence of modulated charged surfaces in narrow confinements. *J. Fluid Mech.* **776**, 390–429.

MARK, D., HAEBERLE, S., ROTH, G., VON STETTEN, F. & ZENGERLE, R. 2010 Microfluidic lab-on-a-chip platforms: requirements, characteristics and applications. *Chem. Soc. Rev.* **39** (3), 1153–1182.

MASLIYAH, J. H. & BHATTACHERJEE, S. 2006 *Electrokinetic and Colloid Transport Phenomena*. Wiley-Interscience.

MAYNES, D. & WEBB, B. W. 2003 Fully developed electro-osmotic heat transfer in microchannels. *Intl J. Heat Mass Transfer* **46** (8), 1359–1369.

MAZUMDER, B. S. & DAS, S. K. 1992 Effect of boundary reaction on solute dispersion in pulsatile flow through a tube. *J. Fluid Mech.* **239**, 523–549.

MOGENSEN, K. B., GANGLOFF, L., BOGGILD, P., TEO, K. B. K., MILNE, W. I. & KUTTER, J. P. 2009 Carbon nanotubes integrated in electrically insulated channels for lab-on-a-chip applications. *Nanotechnology* **20** (9), 95503.

MORIKAWA, K., MAWATARI, K., KATO, M., TSUKAHARA, T. & KITAMOTRI, T. 2010 Streaming potential/current measurement system for investigation of liquids confined in extended-nanospace. *Lab on a Chip* **10** (7), 871–875.

MOYERS-GONZALEZ, M., OWENS, R. G. & FANG, J. 2008 A non-homogeneous constitutive model for human blood. Part 1. Model derivation and steady flow. *J. Fluid Mech.* **617**, 327–354.

MUKHERJEE, S., DHAR, J., DASGUPTA, S. & CHAKRABORTY, S. 2019 Patterned surface charges coupled with thermal gradients may create giant augmentations of solute dispersion in electro-osmosis of viscoelastic fluids. *Proc. R. Soc. Lond.* A **475** (2221), 20180522.

MUKHERJEE, S., DAS, S. S., DHAR, J., CHAKRABORTY, S. & DASGUPTA, S. 2017*a* Electroosmosis of viscoelastic fluids: role of wall depletion layer. *Langmuir* **33** (43), 12046–12055.

MUKHERJEE, S., GOSWAMI, P., DHAR, J., DASGUPTA, S. & CHAKRABORTY, S. 2017*b* Ion-size dependent electroosmosis of viscoelastic fluids in microfluidic channels with interfacial slip. *Phys. Fluids* **29** (7), 72002.

NG, C.-O. 2006 Dispersion in steady and oscillatory flows through a tube with reversible and irreversible wall reactions. *Proc. R. Soc. Lond.* A **462** (2066), 481–515.

NG, C.-O. & YIP, T. L. 2001 Effects of kinetic sorptive exchange on solute transport in open-channel flow. *J. Fluid Mech.* **446**, 321–345.

NGUYEN, T., XIE, Y., DE VREEDE, L. J., VAN DEN BERG, A. & EIJKEL, J. C. T. 2013 Highly enhanced energy conversion from the streaming current by polymer addition. *Lab on a Chip* **13** (16), 3210.

OHNO, K., TACHIKAWA, K. & MANZ, A. 2008 Microfluidics: applications for analytical purposes in chemistry and biochemistry. *Electrophoresis* **29** (22), 4443–4453.

OLIVARES, M. L., VERA-CANDIOTI, L. & BERLI, C. L. A. 2009 The EOF of polymer solutions. *Electrophoresis* **30** (5), 921–929.

OWENS, R. G. 2006 A new microstructure-based constitutive model for human blood. *J. Non-Newtonian Fluid Mech.* **140** (1–3), 57–70.

PAN, S., NGUYEN, D. A., DÜNWEG, B., SUNTHAR, P., SRIDHAR, T. & RAVI PRAKASH, J. 2018 Shear thinning in dilute and semidilute solutions of polystyrene and DNA. *J. Rheol.* **62** (4), 845–867.

PROBSTEIN, R. F. 1994 *Physicochemical Hydrodynamics: An Introduction*. Wiley.

RAJ, M. K., DASGUPTA, S. & CHAKRABORTY, S. 2017 Hydrodynamics in deformable microchannels. *Microfluid. Nanofluid.* **21** (4), 70.

RAJ, P. M., SARKAR, S., CHAKRABORTY, S., PHANIKUMAR, G., DUTTA, P. & CHATTOPADHYAY, K. 2002 Modelling of transport phenomena in laser surface alloying with distributed species mass source. *Intl J. Heat Fluid Flow* **23** (3), 298–307.

RANA, U., CHAKRABORTY, S. & SOM, S. K. 2014 Thermodynamics of premixed combustion in a heat recirculating micro combustor. *Energy* **68**, 510–518.

REPPERT, P. M. 2003 Temperature-dependent streaming potentials: 1. Theory. *J. Geophys. Res.* **108** (B11), 2546.

REVIL, A., PEZARD, P. A. & GLOVER, P. W. J. 2003 Streaming potential in porous media: 1. Theory of the zeta potential. *J. Geophys. Res.* **104** (B9), 20033–20048.

REVIL, A., SCHWAEGER, H., CATHLES, L. M. & MANHARDT, P. D. 1999 Streaming potential in porous media: 2. Theory and application to geothermal systems. *J. Geophys. Res.* **104** (B9), 20021–20031.

SADEGHI, A., YAVARI, H., SAIDI, M. H. & CHAKRABORTY, S. 2011 Mixed electroosmotically and pressure-driven flow with temperature-dependent properties. *J. Thermophys. Heat Transfer* **25** (3), 432–442.

SÁNCHEZ, S., ASCANIO, G., MÉNDEZ, F. & BAUTISTA, O. 2018 Theoretical analysis of non-linear Joule heating effects on an electroosmotic flow with patterned surface charges. *Phys. Fluids* **30** (11), 112002.

SANDBAKK, K. D., BENTIEN, A. & KJELSTRUP, S. 2013 Thermoelectric effects in ion conducting membranes and perspectives for thermoelectric energy conversion. *J. Membr. Sci.* **434**, 10–17.

SARKAR, S., RAJ, P. M., CHAKRABORTY, S. & DUTTA, P. 2002 Three-dimensional computational modeling of momentum, heat, and mass transfer in a laser surface alloying process. *Numer. Heat Transfer* A **42** (3), 307–326.

SILVA, A. F., ALVES, M. A. & OLIVEIRA, M. S. N. 2017 Rheological behaviour of vitreous humour. *Rheol. Acta* **56** (4), 377–386.

SINTON, D., ESCOBEDO-CANSECO, C., REN, L. & LI, D. 2002 Direct and indirect electroosmotic flow velocity measurements in microchannels. *J. Colloid Interface Sci.* **254** (1), 184–189.

SMITH, R. 1982 Contaminant dispersion in oscillatory flows. *J. Fluid Mech.* **114**, 379–398.

SOUNART, T. L. & BAYGENTS, J. C. 2007 Lubrication theory for electro-osmotic flow in a non-uniform electrolyte. *J. Fluid Mech.* **576**, 139–172.

STONE, H. A., STROOCK, A. D. & AJDARI, A. 2004 Engineering flows in small devices: microfluidics toward a lab-on-a-chip. *Annu. Rev. Fluid Mech.* **36** (1), 381–411.

STROOCK, A. D., DERTINGER, S. K. W., AJDARI, A., MEZIC, I., STONE, H. A. & WHITESIDES, G. M. 2002 Chaotic mixer for microchannels. *Science* **295** (2002), 647–651.

SUGIOKA, H. 2010 Chaotic mixer using electro-osmosis at finite Péclet number. *Phys. Rev.* E **81** (3), 036306.

TANG, G. Y., YANG, C., CHAI, C. J. & GONG, H. Q. 2003 Modeling of electroosmotic flow and capillary electrophoresis with the joule heating effect: the Nernst–Planck equation versus the boltzmann distribution. *Langmuir* **19** (26), 10975–10984.

TAYLOR, G. 1953 Dispersion of soluble matter in solvent flowing slowly through a tube. *Proc. R. Soc. Lond.* A **219** (1137), 186–203.

TIRTAATMADJA, V., MCKINLEY, H. G. & COOPER-WHITE, J. J. 2006 Drop formation and breakup of low viscosity elastic fluids: effects of molecular weight and concentration. *Phys. Fluids* **18** (4), 043101.

VAN DEEMTER, J. J., ZUIDERWEG, F. J. & KLINKENBERG, A. 1956 Longitudinal diffusion and resistance to mass transfer as causes of nonideality in chromatography. *Chem. Engng Sci.* **5** (6), 271–289.

VAN DER HEYDEN, F. H., BONTHUIS, D. J., STEIN, D., MEYER, C. & DEKKER, C. 2007 Power generation by pressure-driven transport of ions in nanofluidic channels. *Nano Lett.* **7** (4), 1022–1025.

VAN DER HEYDEN, F. H. J., STEIN, D. & DEKKER, C. 2005 Streaming currents in a single nanofluidic channel. *Phys. Rev. Lett.* **95** (11), 116104.

VENDITTI, R., XUAN, X. & LI, D. 2006 Experimental characterization of the temperature dependence of zeta potential and its effect on electroosmotic flow velocity in microchannels. *Microfluid. Nanofluid.* **2** (6), 493–499.

WATSON, E. J. 1983 Diffusion in oscillatory pipe flow. *J. Fluid Mech.* **133**, 233–244.

WHITESIDES, G. M. 2006 The origins and the future of microfluidics. *Nature* **442** (7101), 368–373.

WÜRGER, A. 2008 Transport in charged colloids driven by thermoelectricity. *Phys. Rev. Lett.* **101** (10), 108302.

WÜRGER, A. 2010 Thermal non-equilibrium transport in colloids. *Rep. Prog. Phys.* **73** (12), 126601.

XUAN, X. 2008 Joule heating in electrokinetic flow. *Electrophoresis* **29** (1), 33–43.

XUAN, X. C., XU, B., SINTON, D. & LI, D. Q. 2004 Electroosmotic flow with Joule heating effects. *Lab on a Chip* **4** (3), 230–236.

ZENG, S., CHEN, C. H., MIKKELSEN, J. C. & SANTIAGO, J. G. 2001 Fabrication and characterization of electroosmotic micropumps. *Sensors Actuators* B **79** (2–3), 107–114.

ZHANG, J. B., HE, G. W. & LIU, F. 2006 Electro-osmotic flow and mixing in heterogeneous microchannels. *Phys. Rev.* E **73** (5), 056305.

ZHANG, W., WANG, Q., ZENG, M. & ZHAO, C. 2019 Thermoelectric effect and temperature-gradient-driven electrokinetic flow of electrolyte solutions in charged nanocapillaries. *Intl J. Heat Mass Transfer* **143**, 118569.

ZHAO, C. & YANG, C. 2011 Electro-osmotic mobility of non-Newtonian fluids. *Biomicrofluidics* **5** (1), 014110.

ZHAO, C. & YANG, C. 2013 Electrokinetics of non-Newtonian fluids: a review. *Adv. Colloid Interface Sci.* **201–202**, 94–108.

ZHAO, H. 2011 Streaming potential generated by a pressure-driven flow over superhydrophobic stripes. *Phys. Fluids* **23** (2), 22003.

ZHOLKOVSKIJ, E. K. & MASLIYAH, J. H. 2004 Hydrodynamic dispersion due to combined pressure-driven and electroosmotic flow through microchannels with a thin double layer. *Analyt. Chem.* **76** (10), 2708–2718.

ZHOU, Y., XIE, Y., YANG, C. & CHEONG LAM, Y. 2015 Thermal effect on microchannel electro-osmotic flow with consideration of thermodiffusion. *Trans. ASME J. Heat Transfer* **137** (9), 91023.